STUDY OF RANDOM WAVE PHENOMENA IN HYPERGOLIC PROPELLANT COMBUSTION

Interim (12 Month) Report SN-87
NASA Contract NAS7-467

By E. W. Nadig, E. A. Tkachenko, B. P. Breen
Dynamic Science, A Division of Marshall Industries

30 June 1967

NATIONAL AERONAUTICS AND SPACE ADMINISTRATION

FOREWORD

This interim report was prepared for NASA Jet Propulsion Laboratory. Project Monitor on this contract is Richard M. Clayton, Liquid Propulsion Section of Jet Propulsion Laboratory, California Institute of Technology, Pasadena, California.

This effort was conducted for the Contract NAS 7-467 for the period May 1, 1966 to May 30, 1967. Dynamic Science number assigned to this report is SN-87.

This is an interim report (12 months) covering a continuing research program being conducted to develop a meaningful model of random wave phenomena occurring with hypergolic propellants during starting transients and during steady operation.

TABLE OF CONTENTS

I. SUMMARY

High amplitude pressure waves (pressure spikes) associated with vacuum engine starting transients, and pressure pulses (pops) occurring during steady state operation of hypergolic liquid rocket engines can be totally or partly detrimental to the rocket engine. The purpose of this research is to describe the conditions which, if present in a rocket combustion chamber during starting transient and during steady operation, will produce the observed pressure disturbances. Thus, the mechanism by means of which pressure spikes and pops develop are studied, however, the definition and verification of the pressure spike mechanism is emphasized. Both theoretical studies and laboratory experiments are utilized to accomplish this end.

A detailed model is being developed which interrelates equations involving: 1) transient flow rate, 2) chamber pressurization, 3) preignition chemistry and delay, and 4) detonation processes. The model will determine conditions which exist in the chamber until ignition and, ideally, will quantitatively predict the magnitude and time of occurrence of the overpressure.

To date, certain of the individual system processes of the model have been formulated and their solution has been obtained with the aid of a digital computer, whereas other processes still require additional analysis and experimentation.

II. INTRODUCTION

The importance of gaining a better understanding of starting transients and steady-state operation in hypergolic liquid rocket systems is borne out by the many applications of hypergolic propellant systems.

A troublesome, and at the same time, highly complex phenomenon which is observed during engine starting transients is the occurrence of high pressure waves, usually termed pressure spikes. Similarly, pressure distrubances, commonly referred to as pops, are known to occur during steady-state rocket engine operation. Various attempts to explain the nature of these pressure disturbances have been made; however, most of these attempts are qualitative.

The main purpose of this investigation is to develop an analytical model describing combustion chamber conditions during the start transient, although chamber conditions leading to pops are also studied. By necessity, the analytical model is semi-empirical in nature, that is, containing several parameters which are best evaluated from experiment, or empirical correlation.

In order to explain these pressure disturbances, it has generally been assumed that explosions of accumulated propellant masses are the cause of the observed pressure waves. As the result of more recent experimental studies, it was found that under certain conditions, detonable chemical reaction intermediates accumulate in the combustion chamber. This fact, evidently, adds a further complicating aspect to the quantitative description of pressure spikes.

It would be clearly presumptuous to claim that a model based on theory alone could provide results of highly practical value to designers in order to eliminate or control spiking. Thus, the intent and contribution of the present study is to provide an analytical framework which will make possible parametric studies, showing which parameters affect chamber behavior most significantly and thus, will suggest the measurement of these parameters.

The present model is one-dimensional and is based on time dependent differential equations formulating physical and chemical processes

governing chamber conditions. The sets of equations consist of:

(1) Transient flow equations with time dependent resistance, inertance, and flow capacitance.

(2) Vaporization, freezing, and pressurization equations.

(3) Chemical kinetic equations including concentration and temperature dependence.

(4) Detonation equations for a multiphase system.

The actual solution of these equations is carried out numerically by a finite difference method and the computer program is arranged such that each of the cited sets of equations is treated as one unit. It is clear that the hydrodynamic and physiochemical equations are interdependent. For example, calculation of chamber pressure requires knowledge of the injection flow rate and the entering liquid and vapor mass fraction, temperature, preignition chemistry with related gas production, propellant vaporization rate, and nozzle exhaust losses. Changes in chamber pressure, in turn, influence the injection flow rate.

In the ensuing discussion the problem of pressure spikes and pops will be defined and a background will be provided in terms of a literature review and some order of magnitude calculations. The ignition spiking analysis will be discussed in detail and the results of certain parametric computational studies will be presented.

III. PROBLEM DEFINITION

Discussion

The pressure spike phenomenon is characterized by a sudden rise in combustion chamber pressure during the ignition process in a rocket engine. Pressure rise rates of the order of 200 psia/μ sec are observed, and peak pressures as high as 5000 psia have been recorded within the combustion chamber. Such behavior, represented schematically in the sketch below, is especially likely to occur at vacuum engine ignition.

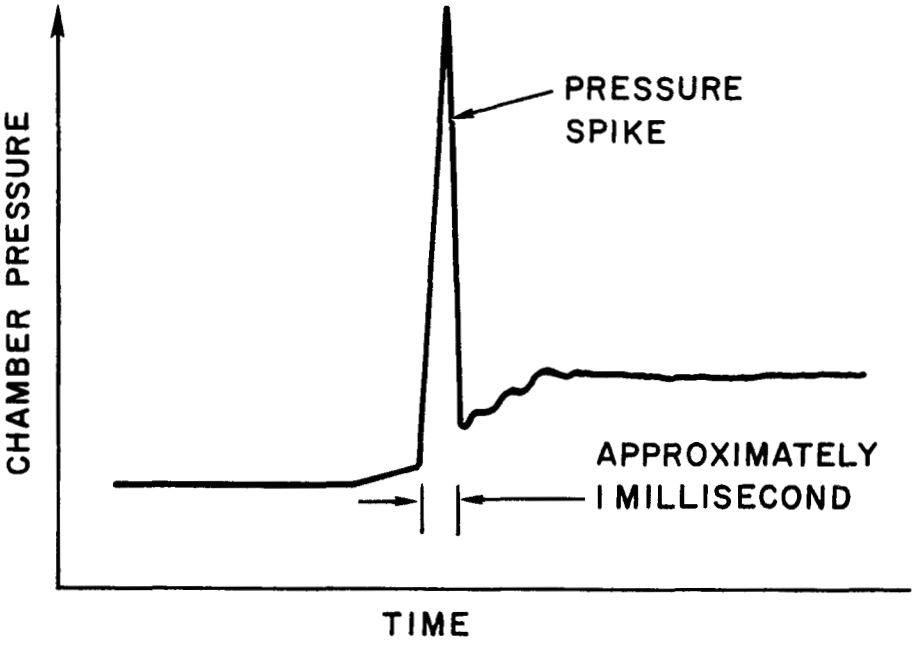

Although a considerable variance of the pressure spike amplitude is observed, the duration of a pressure spike is consistently of the order of one millisecond. The overall pressure spike has been resolved experimentally into a fine structure, namely, into several separate pressure peaks, each occurring over a duration of 70 to 100 μsec.

In contrast to the high amplitude (potentially destructive) pressure spikes associated with starting transients, the relatively low level pops appear to have been studied to a lesser degree. The characteristics of a chamber pressure pop resemble those connected with nonlinear, pulse or bomb induced disturbances. For example, the similarities consist of the steep-fronted pressure rise, the resulting maximum overpressure, and the damping characteristics. Both structural-hydrodynamic and physical-chemical effects have been assumed to have a part in popping. Experimentally it has been found that popping is influenced by the propellant combination, mixture ratio, and manufacturing peculiarities of a specific injector.

In general, any propellant system can exhibit overpressures at particular operating conditions. In the following table are listed hypergolic systems which are known to exhibit transient overpressures.

TABLE I. HYPERGOLIC PROPELLANT SYSTEMS EXHIBITING SPONTANEOUS PRESSURE DISTURBANCES

Propellant Systems	Spiking	Popping
1. Nitrogen tetroxide - Aerozine 50	x	x
2. Nitrogen tetroxide - Monomethylhydrazine	x	x
3. Nitrogen tetroxide - Hydrazine	x	
4. Nitrogen tetroxide - Unsymmetrical Dimethylhydrazine	x	
5. Nitric acid - Ethylenediamine	x	
6. Nitric acid - Triethylamine	x	
7. Nitric acid - Hydrazine	x	
8. Nitric acid - Unsymmetrical Dimethylhydrazine	x	
9. Nitric acid - Dimethylaminoethanol	x	
10. Nitrogen tetroxide - 50% hydrazine - 50% monomethylhydrazine	x	x

These chemical systems are known to form unstable intermediate compounds under low temperature--low pressure conditions. It is possible that these intermediate compounds play an important role in the spiking phenomenon.

The literature dealing with overpressure phenomena in the cited hypergolic propellant systems is quite extensive. Rather than provide a complete listing of references treating the problem, only the most pertinent and most illustrative will be presented. The aim is to supplement the problem definition by listing and commenting on existing experimental work and existing hypotheses.

Literature Review

Reference 1. - R. M. Knox, S. J. Minton, and E. B. Zwick, Space Ignition, AIAA Second Propulsion Joint Specialist Conference, Colorado Springs, Colorado, June 13-17, 1966.

Knox, Minton, and Zwick report very recent information on pressure spikes. They group pressure spikes under low backpressure conditions into three groups:

(1) Vapor phase detonations with resulting peak pressures of less than 1500 psi. Frequently, smooth ignition occurs without an indication of detonation. No case of engine damage resulting from this type of ignition has ever been observed at Marquardt (no theoretical calculations are given to support the fact that a vapor phase detonation occurs.)

(2) Large pressure which can damage an engine has been traced to a condensed phase explosion. This type of explosion is believed to be due to the accumulation of frozen fuel on the wall of the chamber. Thus, if at the start of the next pulse the oxidizer valve is opened before the fuel valve, the oxidizer is believed to form explosive compounds with the frozen fuel in the engine. Residual frozen fuel can be present when the engine is started as a result of emptying from the dribble volumes, as a result of a leaky valve, and as a result of improper test procedures.

(3) Propellant manifold explosions - which do not occur under space conditions.

Reference 2. - S. J. Minton and E. B. Zwick, Hypergolic Combustion Initiated at Low Pressure, Aviation Space Conference of the American Society of Mechanical Engineers, March 1965, 47 pp.

Reference 3. - J. J. Kappl and R. M. Knox, Altitude Ignition of Hypergolic Bipropellant Rockets, Marquardt Corporation, 1965, 40 pp.

These references present information obtained in the Marquardt Corporation's program to investigate the nature and prevention of high pressure spikes during ignition of 50% hydrazine-50% UDMH (Aerozine 50) and nitrogen tetroxide fueled rockets at low ambient pressures. Significant experimental results are:

(1) The magnitudes of the peak pressure follow a random distribution.

(2) The peak pressure produced seems to bear no relationship to the time delay but is randomly distributed.

(3) The highest peak pressures occur with a 4 millisecond oxidizer lead.

(4) The effect of increasing the propellant temperature is to shift the distribution of pressure peaks to lower values.

Photographs of the ignition process are presented which are claimed to be suggestive of an initial deflagration followed by a detonation of the remaining material.

Reference 4. - M. L. J. Bernard and J. Dufour, On the Existence of Detonation Conditions in the Combustion of Some Nitric Acid Propellants, Eighth International Symposium on Combustion, 1960, pp. 1074-1084.

Bernard and Dufour conclude that in the nitric acid-fuel (amines, alcohols, hydrazines, etc.) system there is a close relationship between the formation of unstable intermediate compounds and pressure spikes. Various explosive nitrates were found on the chamber walls of the test apparatus used. In the nitric acid-furfuyl alcohol system the rate of pressure rise for a normal ignition is 17.8 $Kg/cm^2/msec$ or 252 psi/msec. The temperature rise was estimated at $100^{\circ}C$ over the entire ignition delay period. These pressure and temperature rises are believed (by Bernard and Dufour) sufficient to cause

deflagration and detonation respectively, of an explosive nitrate. A Fastax film study showed that an "abnormal" ignition (pressure spike) occurred when the chamber was first filled with vapors causing the entire chamber to light up at once. Contrasted to this was a "normal" ignition which occurred at several points in the chamber at the same time. (This suggests that perhaps a vapor phase detonation is initiated by a local hot spot or perhaps an explosive intermediate compound.)

Reference 5. - R. E. Martens, Investigation of the Hypergolic Ignition Spike Phenomena, McDonnell Aircraft Corporation, Internal Report, 27 pp.

Martens carried out an experimental investigation of vacuum firings of a 25 lb. thrust engine using nitrogen tetroxide and monomethylhydrazine. The preignition accumulation of liquid oxidizer on the thrust chamber walls, verified experimentally, is claimed to be the source of the severe ($\geq$ 400 psia) ignition spike phenomena. Upon fuel injection an overspray collects on this coating in a small segment of the chamber. Following a vapor phase ignition, originating in the uncollected propellants, these accumulated propellants react providing a locally high pressure. This high pressure region, bounded on both sides by a lower pressure, generates a wave system analogous to that of a dual diaphragm closed shock tube.

A simplified ignition spike analytical model incorporating the experimental findings was developed. The model was used to calculate the relationship between maximum ignition spike pressures and oxidizer lead time which duplicated the experimental results.

Severe spikes were only encountered during oxidizer lead starts at vacuum conditions and their severity increased with decreasing propellant and hardware temperature.

In the McDonnell injector configuration the orientation of the oxidizer orifices was such that the oxidizer streams were canted outwards. Only an oxidizer to fuel ratio of 1.6 was used in the tests.

On the fuel lead side severe spikes were not encountered, only gradual

pressure rises to approximately 400 psia were measured. On the oxidizer lead side, the ignition spike level was found to increase with lead time until a plateau was reached. This plateau, which persists for approximately 14 to 15 milliseconds, is then terminated by a regime in which ignition spikes could not be generated.

Reference 6. - Norm Chaffee, NASA Manned Spacecraft Center, Houston, Texas, verbal communication.

Mr. Chaffee reports that the Manned Spacecraft Center is carrying out an experimental investigation of the spiking problem using the Marquardt engine. He mentions that a condensed phase residue is present in the chamber after firing and that hydrazinium nitrate ($N_2H_5NO_3$) was identified.

Reference 7. - Thiokol Chemical Corporation, Reaction Motors Division, Hypergolic Ignition at Reduced Pressures, Technical Report No. AFRPL-TR-64-175, December 1964.

Reaction Motors Division investigated the effect of several parameters on the ignition delay of propellant combinations containing N_2O_4 and IRFNA as the oxidizers and unsymmetrical dimethyl hydrazine, monomethyl hydrazine and 50% UDMH-50% N_2H_4 as the fuels. Parameters investigated were injection velocity, impingement length and angle, manifold feed configuration, propellant temperature, and ambient pressure. It was found that ambient pressure alone had the only significant effect on the ignition delay characteristics of all the injector and environmental parameters investigated in unconfined impingement tests.

Reference 8. - B. R. Lawver, and J. J. Kappl, Effect of Additives on Altitude Hypergolic Ignition, AIAA Second Propulsion Joint Specialist Conference, Colorado Springs, Colorado, June 13-17, 1966, 31 pp.

This work experimentally evaluated the effectiveness of selected fuel additives in eliminating or reducing altitude ignition pressure spikes in the propellant combination N_2O_4/Aerozine 50. Eleven different additives were mixed with the fuel in the proportion of 1% by weight. None of the chemical additives

tested were effective in reducing the maximum pressure spike experienced with N_2O_4/Aerozine 50. However, three of the additives significantly increased both the mean and the maximum pressure spike level, thus indicating that additives can influence the altitude ignition process.

Reference 9. - B. R. Lawver, Effect of Ignition O/F on Spike Pressure Distribution, Marquardt Corporation Interoffice Memo 153-75/49, May 1966.

Results are reported of spike tests conducted with cavitating venturi tubes placed in the propellant valves to shift the O/F at ignition. Certain off O/F ratios resulted in reduced ignition spike pressures.

Reference 10. - G. B. Skinner, W. H. Hedley, and A. D. Snyder, Mechanism and Chemical Inhibition of the Hydrazine-Nitrogen Tetroxide Reaction, ASD-TDR-62-1041, December, 1962.

Reference 11. - H. G. Weiss, A Basic Study of the Nitrogen Tetroxide - Hydrazine Reaction, Dynamic Science, SN-4500, July 1965.

These reports are representative of several that mention the formation of intermediate compounds in the nitrogen tetroxide-hydrazine reaction. Weiss reports the formation of hydrazinium nitrate ($N_2H_5NO_3$) in a low temperature reaction between liquid nitrogen tetroxide and liquid hydrazine. Skinner reports the formation of ammonium nitrate (NH_4NO_3) in a preignition reaction between dilute vapors of N_2O_4 and N_2H_4.

Reference 12. - R. Friedman, W. P. Barnes, and M. Markels, Jr. A Study of Explosions Induced by Contact of Hydrazine - Type Fuels with Nitrogen Tetroxide, ASD-TDR-62-685, September 1962.

Friedman, Barnes, and Markels studied the occasional explosions which result when a hydrazine-type liquid is brought into contact with liquid nitrogen tetroxide with little confinement. The authors propose the existence of an adduct that forms on propellant contact and would be responsible for the explosive reaction. This type of explosion may be related to the pressure spikes observed with this propellant system.

Reference 13. - Henry E. Perlee and Theodore Christos, Summary of Hypergolic Ignition Spike Phenomena, U. S. Department of the Interior, Bureau of Mines Final Report No. 3982, April 8, to December 31, 1965.

The Bureau of Mines carried out a literature survey of hypergolic ignition spike phenomena for the MSC in Houston, Texas. One hundred and sixty three articles are reviewed including some of these mentioned above. Topics covered include: physics of spray formation, hydrodynamics of fluid streams, jets in initially low pressure environments, volatile liquid flow in initially low pressure piping, heterogeneous pipe flow, hydrodynamic instability criteria of liquid jets, single particle physics, cooperative phenomena, drop kinematics, transport phenomena, physics of sprays, chemistry of combustion, ignition, flame propagation, and gas dynamics. It would serve no useful purpose to comment on all of these articles here. Most of these refer to physical and chemical processes which take place in an engine and which could have relevance to the hard start phenomena.

Literature on popping is rather scarce. The following reports give experimental results on popping:

Reference 22. - Richard R. Weiss and Raymond D. Klopotek, Experimental Evaluation of the Titan III Transtage Engine Combustion Stability Characteristics, AFRPL-TR-66-51, March, 1966.

Reference 23. - R. R. Weiss, T.J.C. Chew, and Lt. R. D. Klopotek, A Combustion Stability Evaluation of Various Hydrazine and Hydrazine Blend Fuels, Air Force Rocket Propulsion Laboratory, Edwards, California, 42 pp.

This work examined the propellant combinations N_2O_4-A50, N_2O_4-MMH and N_2O_4-Monozine 50. The significant results of the work which involve popping are:

(1) There appears to be no correlation between baffle cracks and the occurrence of popping.

(2) Experimental results did not support the speculation that large amounts of film coolant are a major cause of pops.

(3) N_2O_4-A50 and N_2O_4-MMH appear equally susceptible to the popping type of instability. The N_2O_4/Monozine 50 combination showed a considerable increase in susceptibility to popping.

Reference 24. - R. M. Clayton, Combustion Roughness and Dynamic Stability, Jet Propulsion Laboratory, a section of a future report.

Clayton shows that popping is related to conditions in proximity of the chamber walls. The absence of reactants throughout a substantial space near the chamber boundary and especially in the early reaction zone near the injector was the primary contributor to the absence of popping in a particular engine configuration.

Order of Magnitude Calculations

In order to evaluate the overall relative importance of one-and two-phase detonation and explosion, order of magnitude calculations were carried out applicable to spiking and popping. In order to make these calculations tractable certain simplifying assumptions had to be made. For example, only one-dimensional aspects of detonation and explosion are considered, and complete reaction of the propellants is assumed in the case of two-phase detonation.

Order of Magnitude Calculations Applicable to Spiking. -

Several order of magnitude calculations were made using Marquardt rocket engine data (Refs. 2, 3, 8, and 9).

Gaseous Detonation. The pressure ratio, P_2/P_1, was determined for the case of a vapor phase detonation. The NASA Lewis Chapman-Jouget detonation program was used. This program utilizes a Newton-Raphson iteration procedure to calculate the pressure ratio across the detonation wave. Initial conditions were taken as: initial temperature, 278°K, initial pressures, 2 psia and 4 psia. The resulting pressure ratios were: for 2 psia initial pressure, 72.2; for 4 psia initial pressure, 73.8, based on O/F = 2.

The significance of these results is that these pressure ratios are not high enough to account for pressures obtained in the Marquardt engine (Ref. 9).

Heterogeneous Detonation. Heterogeneous detonation calculations were made using the theory of Ragland, Dabora, and Nicholls (Ref. 14). Assuming that the propellant drops burn completely and that the Chapman-Jouget condition is realized, conservation of mass, momentum, and energy equations are obtained which lead to the following expressions:

$$M_1^2 = 2\left(\frac{\gamma_2^2-1}{\gamma_1-1}\right)\left[\frac{\bar{\alpha}\,\bar{Q}+(\alpha-1)e_\ell}{\alpha\, C_{pl}\, T_1}\right]$$

$$\frac{P_2}{P_1} = \frac{1+\alpha\gamma_1 M_1^2}{1+\gamma_2}$$

where subscript 1 indicates initial conditions, and 2 final conditions, and where

$\alpha = (\rho'_\ell + \rho_1)/\rho_1$

M = Mach number

ρ'_ℓ = mass of liquid per unit volume of mixture

$\bar{Q}$ = heat release due to chemical reaction minus phase change

γ = ratio of specific heats

e_ℓ = internal energy of the liquid.

Order of magnitude calculations were made giving P_2 as a function of O/F ratio.

The NASA-Lewis Chemical Equilibrium program was used to determine the heat of reaction and equilibrium product gases γ_2. The initial temperature, T_1, was taken as 40°F, the initial pressure before spiking as 2 psia (see Figure 1) and $\gamma_1 = 1.4$. For this order of magnitude calculation the internal energy of the liquid and the heat change due to phase transition were neglected. The initial gas density was determined from the ideal gas law at the initial conditions. A quality of 0.043 lb vapor per lb propellant was used (Ref. 2). P_2 was determined as a function of O/F. Figure 1 compares the theoretical results with experimental results obtained at Marquardt, (Ref. 9). Since the pressure ratio, P_2/P_1, varies with quality, Figure 2 was prepared to show the final pressure as a function of quality with initial pressures of 2 psia, 4 psia, and 8 psia as parameters, and an O/F = 2.

In addition to the equations of Ragland, Dabora, and Nicholls (Ref. 14) the following expressions were used in obtaining the curve:

$$f = \frac{M_v}{M_L + M_v}$$

$$p = \frac{M_T}{V_T} RT$$

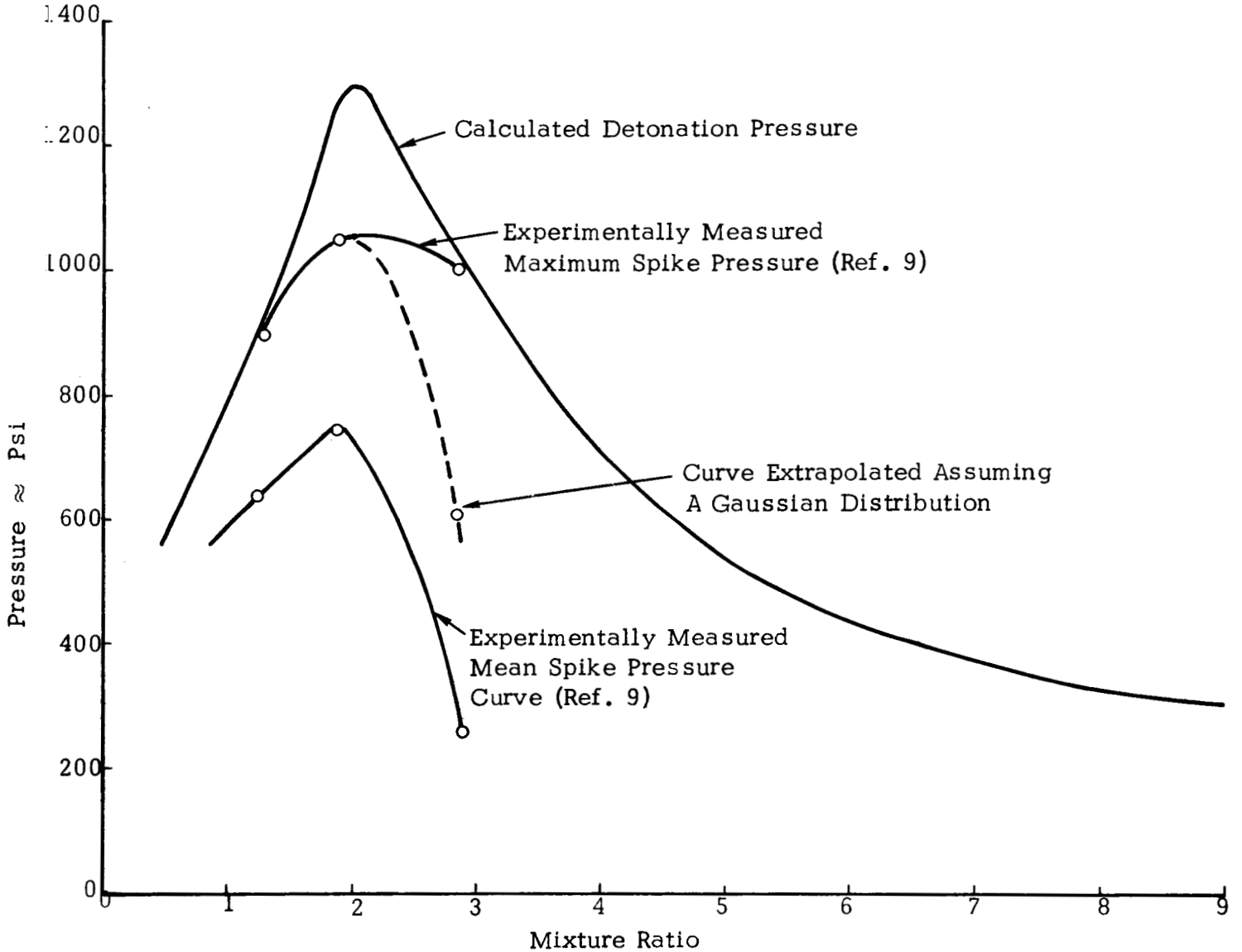

FIGURE 1. Comparison of Ignition Spike Pressure with Calculated Heterogeneous Detonation Pressure.

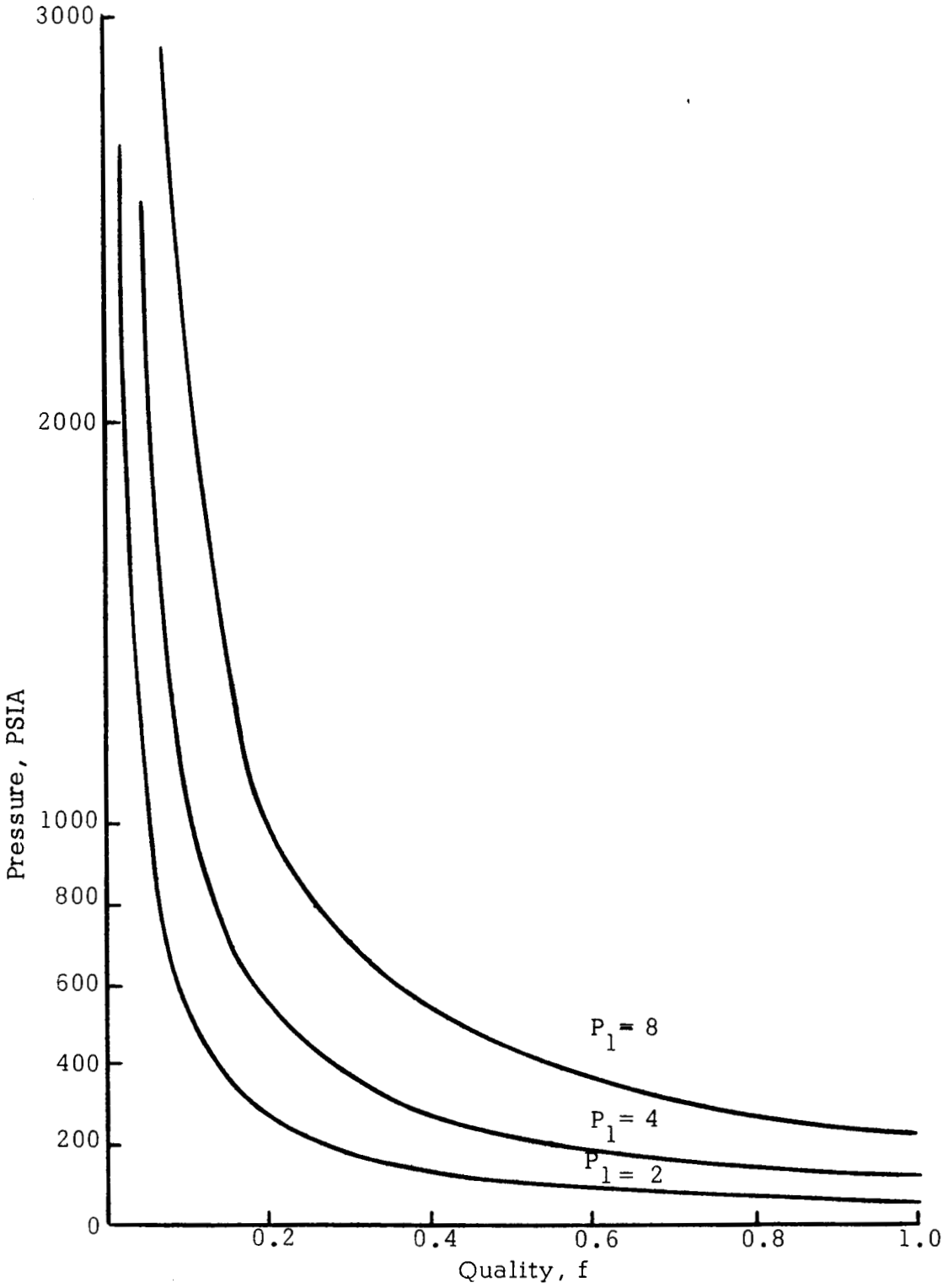

FIGURE 2. PRESSURE VERSUS QUALITY FOR DETONATION

$$\rho_M = \frac{M_\ell + M_v}{V_\ell + V_v}$$

$$\rho_M = \frac{\rho_\ell}{(1-f)+f\,\rho_\ell/\rho_v}$$

where:

f	=	quality of vapor (pounds of vapor per pound of propellant)
α	=	$\frac{\rho_v(1-f)+\rho_\ell}{\rho_v(1-f)+f\rho_\ell}$
M_v	=	mass of vapor
M_L	=	mass of liquid
M_T	=	total mass of propellants
V_T	=	total volume of propellants
V_ℓ	=	volume of liquid
V_v	=	volume of vapor
ρ_ℓ	=	density of liquid
ρ_v	=	density of vapor
ρ_M	=	density of mixture

The results of these order of magnitude calculations, as shown in Figures 1 and 2 indicate that heterogeneous detonation can account for pressure spike amplitudes observed in the Marquardt engine.

Accumulation of Propellant. - A constant volume combustion calculation can be made for the Marquardt engine. Thus, $PV = (W/MW)RT$, where

W	=	0.965×10^{-3} (assuming a 2 millisecond residence time)
R	=	1545 ft lbf/lb mole $^{\circ}$F
T	=	5850°R (from NASA-Lewis program with O/F=2)
V	=	6.28 in.^{3}
MW	=	22 (approximate product gas molecular weight from NASA-Lewis program for O/F=2)

yields P = 760 psia.

An absolute maximum pressure attainable by constant volume combustion may be estimated by assuming no nozzle exit flow throughout the ignition delay period. Thus, on the basis of the above conditions,

$\Delta P/\Delta t$ = 380 psia/millisecond of ignition delay.

For a 5 millisecond ignition delay time one obtains 1900 psia.

For the case of no nozzle exit flow, a pressure is obtained which is in reasonable agreement with some observed Marquardt pressure spikes. However, since the assumption of no nozzle exit flow is unrealistic, the calculated value of 760 psia for the final pressure attained by burning all of the propellant within a 2 millisecond residence time tends to rule out explosion as a mechanism for the hard start observed in the Marquardt engine.

Quality of Marquardt Engine. A value for the quality (pound vapor per pound propellant) was determined from the following data:

Residence time, based on injection velocity	1.5 to 2.0 millisecond
Volume of chamber	6.28 $in.^3$
Cold flow rate	0.483×10^{-3} lbm per millisecond

Thus, ρ_M (density of the mixture) varies between 0.212 lb/ft^3 and 0.266 lb/ft^3. Using the relationship $\rho_M = \rho_L/[(1-f)+f\,\rho_L/\rho_V]$, the quality (f) varies between 0.097 and 0.12 or an average quality of 10.8 per cent.

Explosion. Using the ideal gas law relationship, $P = \rho_M RT$, and the variation of the mixture density with quality, $\rho_M = \rho_\ell/[(1-f)+f\ \rho_L/\rho_V]$, Figure 3 was prepared to show the final pressure, P, as a function of quality, f. An explosion is here defined as instantaneous reaction yielding a pressure calculable from the ideal gas law. A final temperature of 5850°R and an O/F of 2 was used. Figure 3 shows that a relatively high liquid mass fraction is required to yield explosion pressures of the same order of magnitude as are found experimentally.

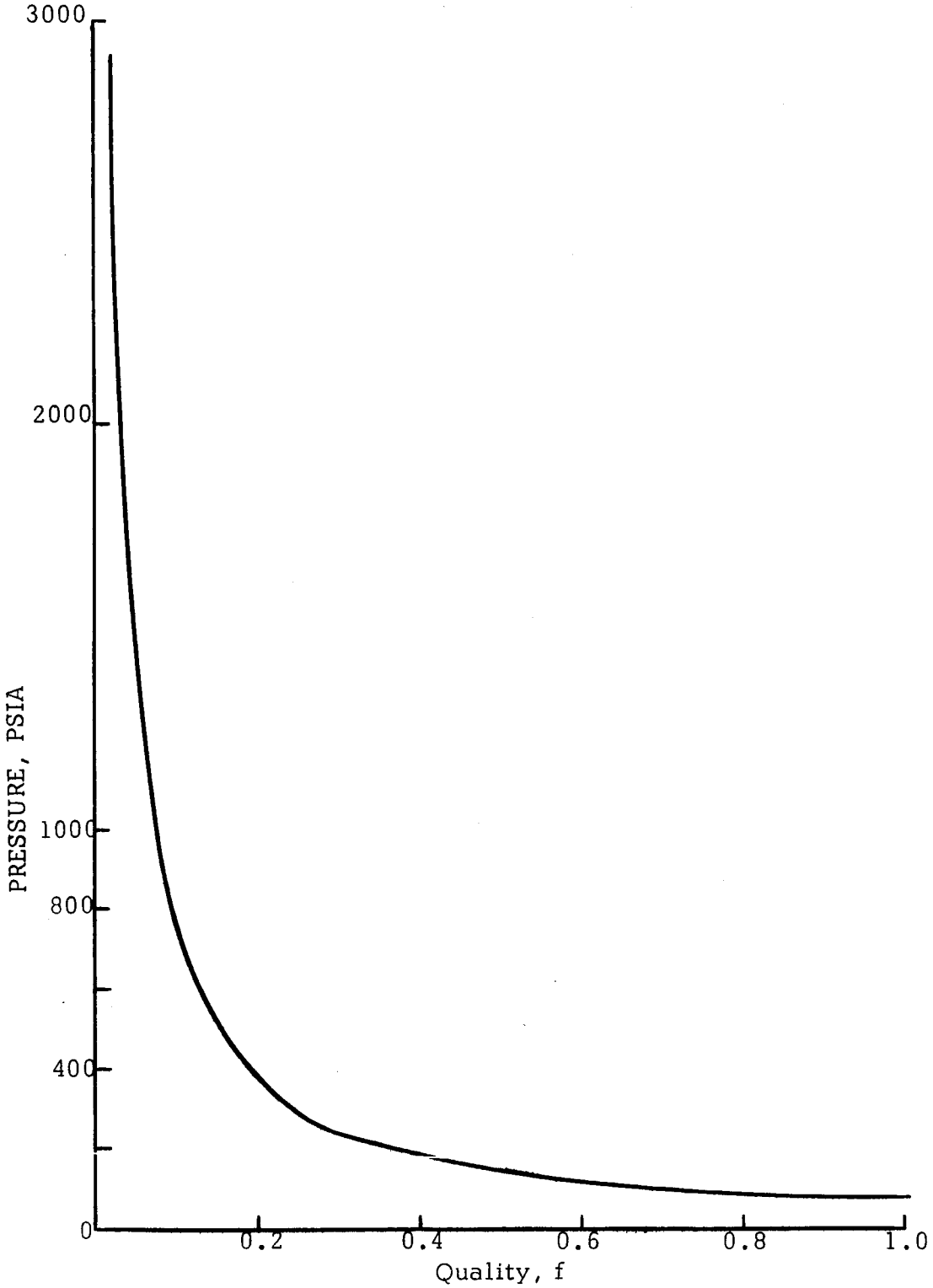

FIGURE 3. PRESSURE VERSUS QUALITY FOR EXPLOSION

Order of Magnitude Calculations Applicable to Popping. -

Heterogeneous Detonation. Employing Dynamic Science's steady-state combustion program in conjunction with Ragland, Dabora, and Nicholl's detonation model (Ref. 14), the detonation pressure ratio was calculated as a function of distance from the injector face. For an O/F = 2 and the N_2O_4/MMH system, the fraction of propellant vaporized as a function of distance from the injector face was calculated using Dynamic Science's combustion program. These data are:

Distance from Face Inches	Per cent Unburnt Material
0.25	93.0
0.50	88.0
0.75	82.0
1.00	78.0
3.00	57.5
5.00	47.0
7.00	40.0
9.00	36.0

The equations:

$$M_1^2 = 2\left(\frac{\gamma_2^2-1}{\gamma_1 - 1}\right) \frac{\bar{Q}}{C_{p1}T_1}$$

and

$$\frac{P_2}{P_1} = \frac{1+\alpha\gamma_1 M_1^2}{1+\gamma_2}$$

were then used. $\bar{Q}$ was modified by taking the heat of reaction from the NASA-Lewis program and multiplying by the per cent of unburned material. The value for γ_1 was taken as 1.4. The specific heat ratio, γ_2, and the steady-state temperature, T_1, were taken from the NASA-Lewis Program. Figure 4 shows the large effect which percent unburnt material and droplet number concentration can have on detonation overpressure near the injector face.

Explosion Phenomena. Besides the magnitude of peak pressures developed in an explosion, the characteristics of pressure decay are of significance. On the basis of published pressure data available at Jet Propulsion Laboratory, various distances from a bomb exploded in the center of a rocket engine, it

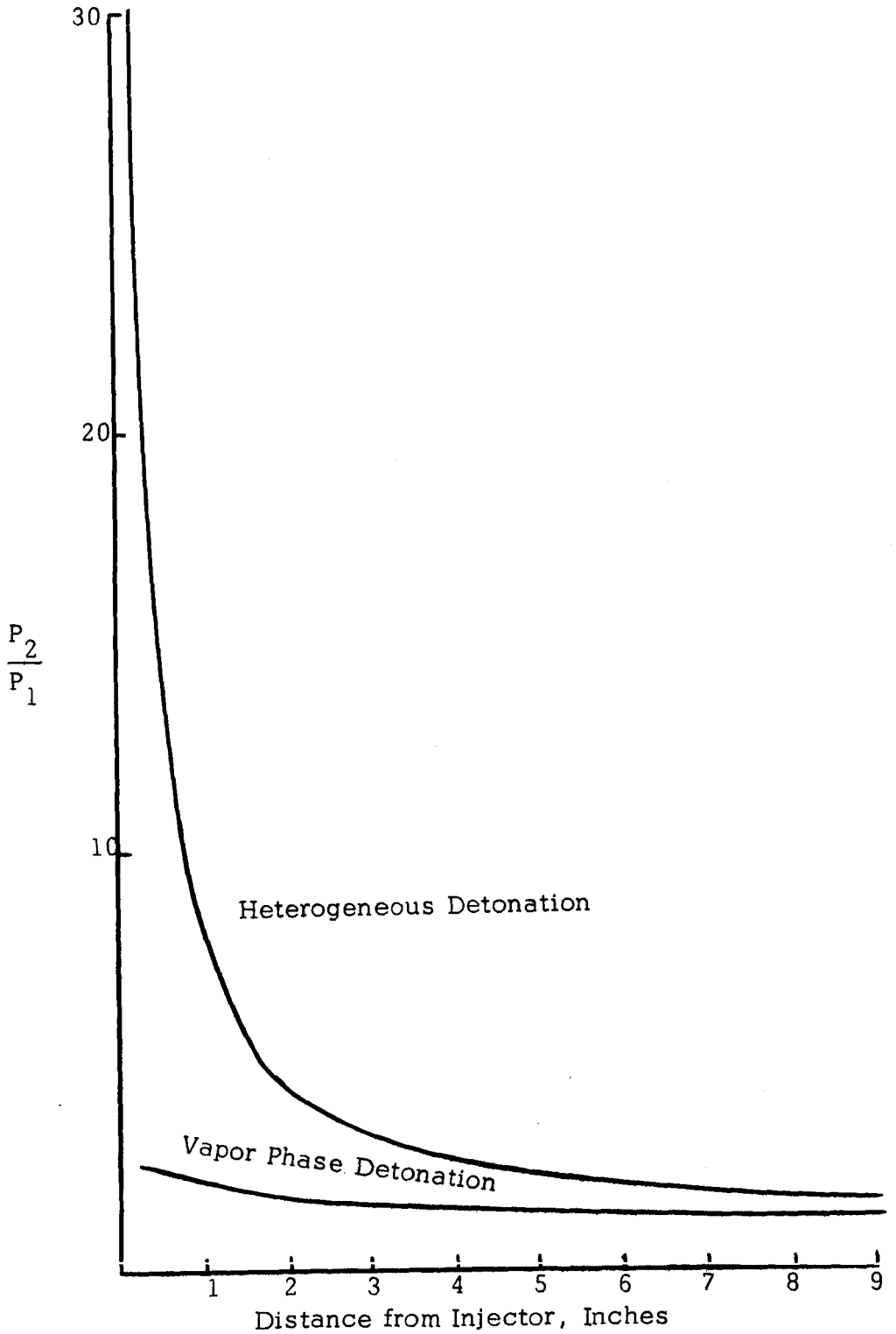

FIGURE 4 . DETONATION PRESSURE RATIO VERSUS DISTANCE

is possible to compare the experimental with isentropic and isothermal expansion. Employing the ideal gas law and the following initial conditions:

weight = 13.5 grains of RDX

grain size = 0.279 in O.D., 1.5 in. long

$R \approx 75$

$T \approx 6000^{\circ}$

one obtains a pressure of 114,000 psia at a radius of 0.49 inches (based on a sphere volume equivalent to the cylinder of explosive). Using this as the initial point,the experimental data are plotted in Figure 5. Also plotted are data for an isothermal expansion (PV = constant) and isentropic expansion (PV^{γ} = constant). According to Figure 5, at radii near 4 inch or greater, the experimental pressure decay curve approximates isothermal expansion.
The results presented in Figure 4 demonstrate the sensitivity of the heterogeneous detonation pressure ratio to distance from the injector. Pressure ratio resulting from a vapor phase detonation, on the other hand, does not vary significantly with distance from the injector.

The significance of the order of magnitude calculations applicable to spiking and popping can be summed up in the following:

(1) Gaseous detonation by itself does not account for peak pressure characteristic of spiking,

(2) Heterogeneous detonation calculations indicate that spike pressures are attainable in regions where the liquid propellant mass fraction is large,

(3) Although constant volume explosion for high liquid to vapor mass ratio yields pressures of spiking magnitude, the closed system assumption for the combustion chamber is unrealistic, and therefore, it is unlikely that explosion accounts for spiking,

(4) Vapor phase and heterogeneous detonation pressures approach nearly the same value at relatively large distances from the injector face, that is, at locations where the liquid mass fraction is low. The magnitudes of these detonation pressures are consistent with overpressures characteristic of pops.

(5) In general, the order of magnitude calculations carried out point to the need for a more detailed modeling of the overpressure phenomena.

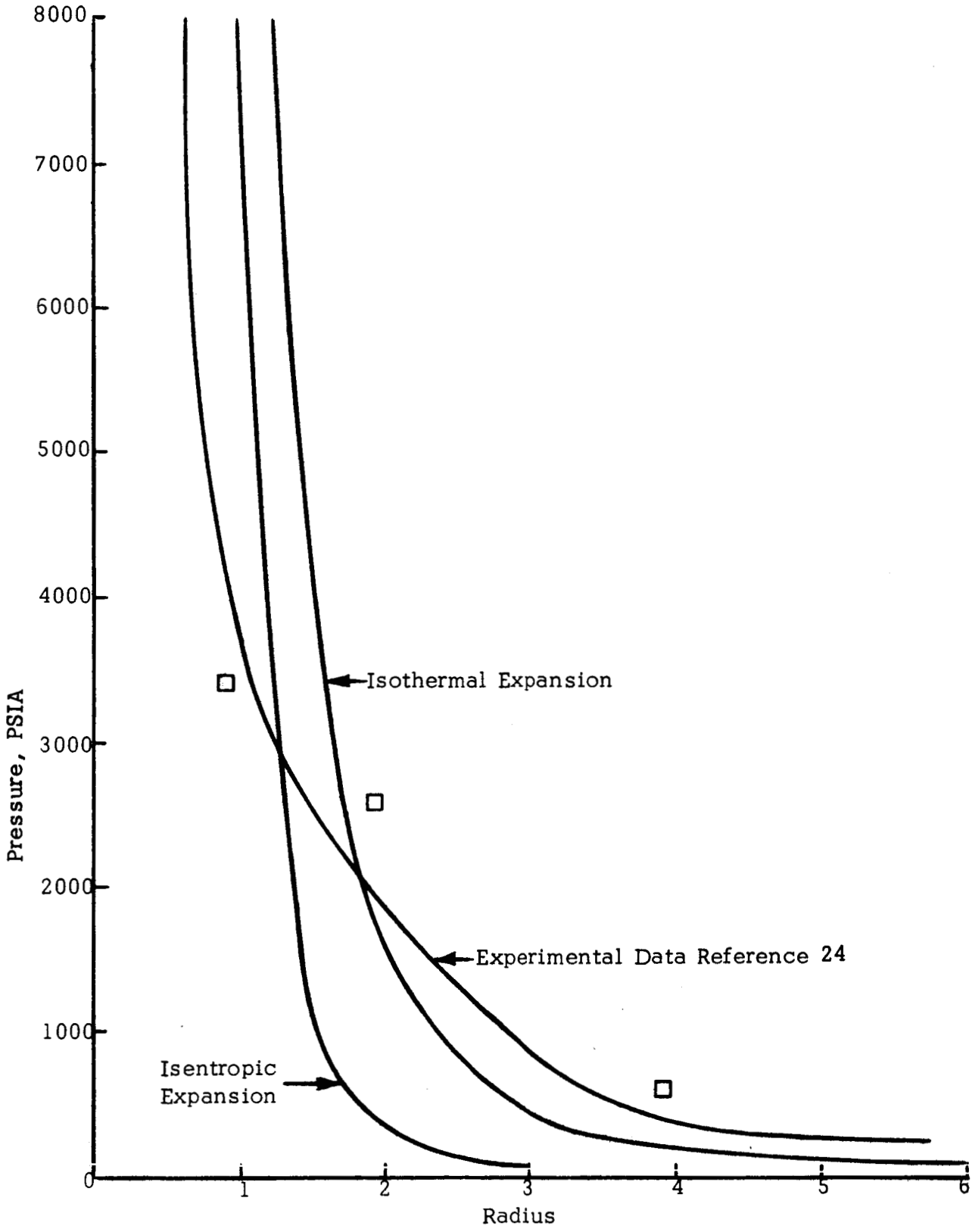

FIGURE 5 . PRESSURE DECAY EXPLOSION CALCULATIONS

The analytical framework to be described in the following section makes possible a more realistic study of the relative importance of various physical and chemical processes involved in hypergolic propellant ignition and combustion.

IV. IGNITION SPIKING ANALYSIS

The pressure spiking phenomenon, as defined in this study, is closely associated with the engine ignition transient. Thus, it is important to consider the ignition sequence variables in order to understand better the complex interaction of the physical and chemical processes.

Discussion of Typical Starting Sequence

Since vacuum or high altitude ignition creates, in practice, the most susceptible condition for spiking, such an ignition sequence (Ref. 8) will be employed to illustrate certain measurable processes taking place in a 100 lb. thrust altitude control engine. In referring to Figure 6, describing a typical altitude ignition sequence, attention should be called to the fact that the various valve signals may be either electrical or real injection lead signals. The actual injection lead, of course, is of particular interest in connection with the ignition delay. In Figure 6, the initial chamber pressure is the cell pressure (≈ 0.5 psia). According to the valve sequencing in Figure 6, the oxidizer leads the fuel by ≈ 5 msec and about 7.5 msec after the oxidizer valve signal, the oxidizer starts to enter the chamber, and the pressure rises to about 1 psia. The fuel starts to enter the chamber about 7.5 msec after the fuel valve signal. In order to describe mathematically the altitude ignition process, it is first necessary to formulate a general framework which takes into account all important variables and their interrelationship. Figures 7, 8, 9, 10, and 11 show schematically the complex interaction of the physical and chemical processes. The chamber pressure $P_c(t)$ is the primary variable which is being described before and during ignition. The chamber pressure is affected by the tank pressure through the four simultaneous and/or parallel systems shown in Figure 7. The four systems being described mathematically are:

(1) The transient flow process (Figure 7),

(2) The chamber pressurization process (Figure 8)

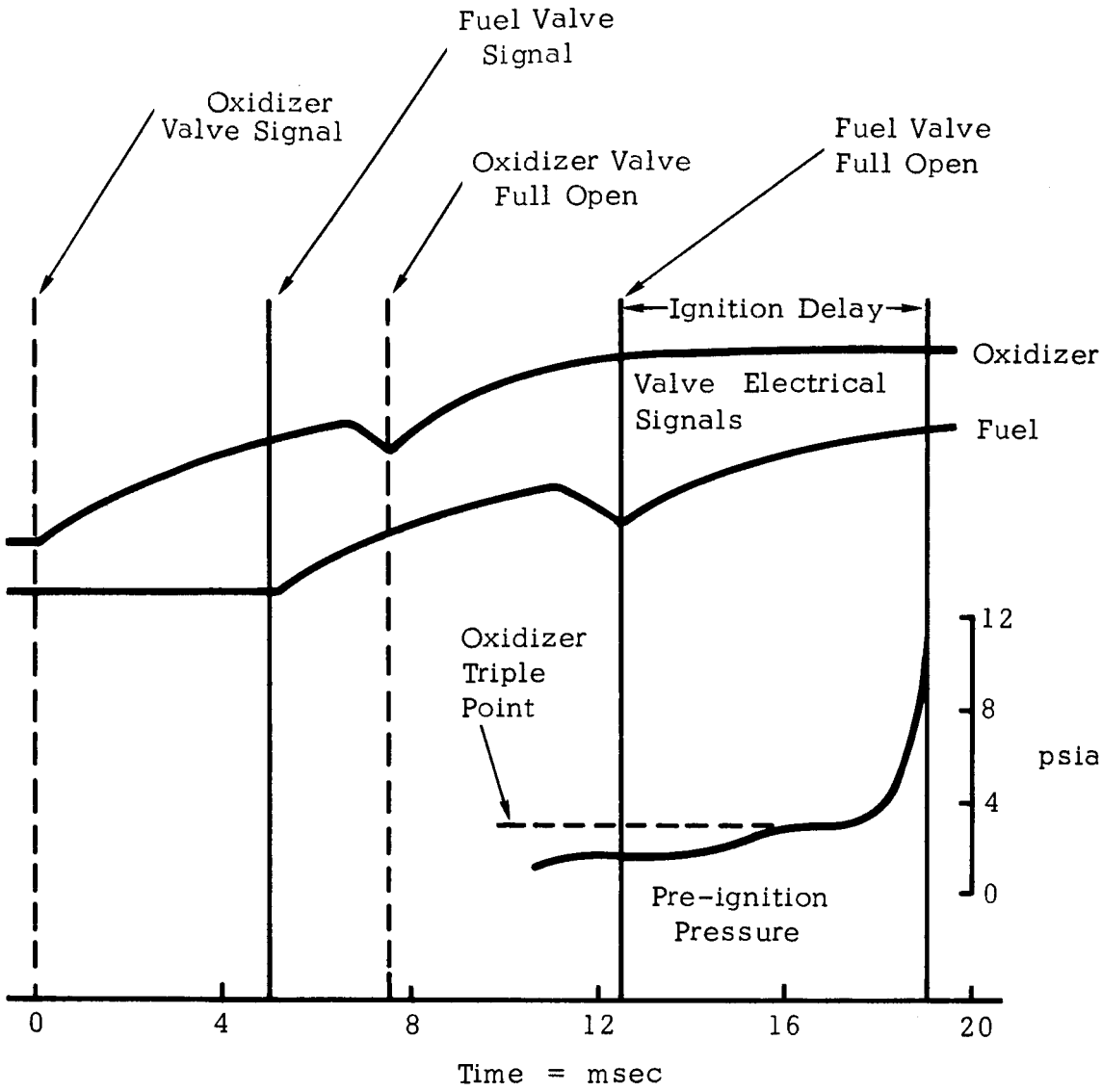

FIGURE 6. Rocket Engine Pre-Ignition Pressure History Data Taken From Reference 8.

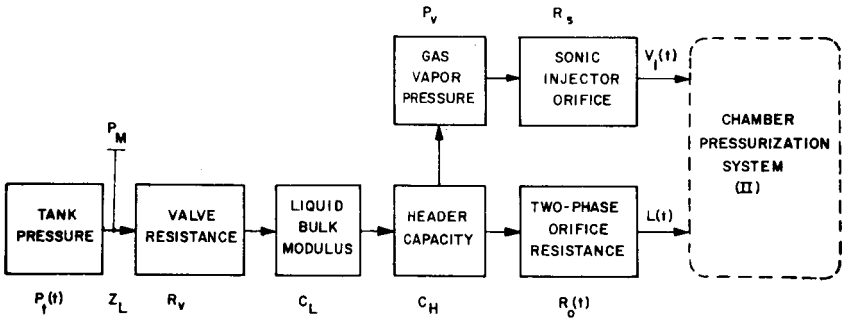

FIGURE 7. TRANSIENT FLOW SYSTEMS (I)

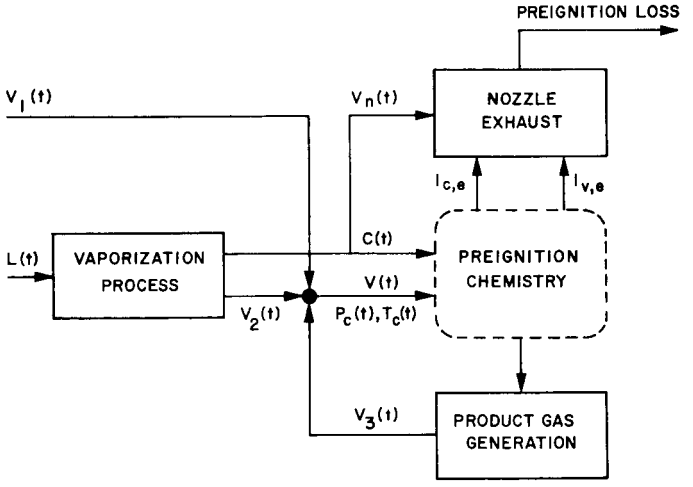

FIGURE 8. CHAMBER PRESSURIZATION SYSTEM (II)

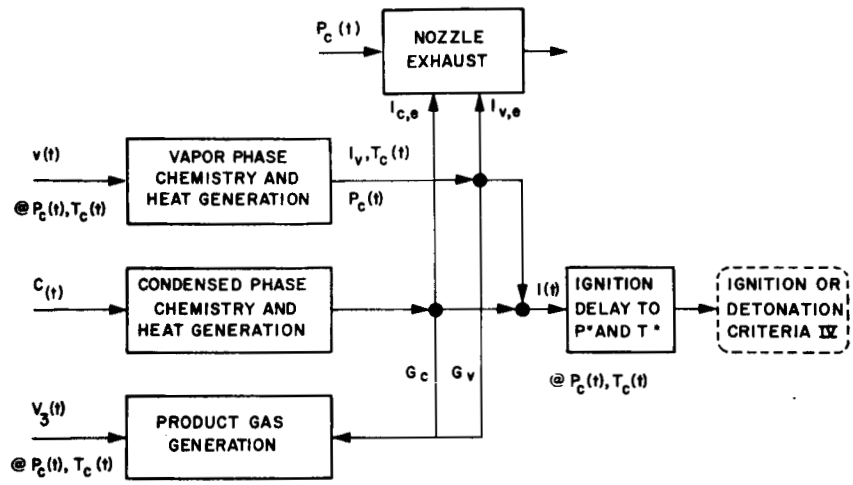

FIGURE 9. PREIGNITION CHEMISTRY SYSTEM (III)

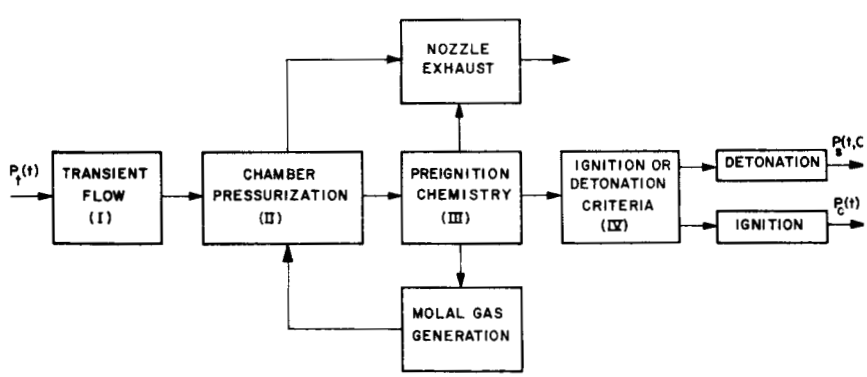

FIGURE 10. ROCKET CHAMBER IGNITION

COMBUSTION/DETONATION SYSTEM

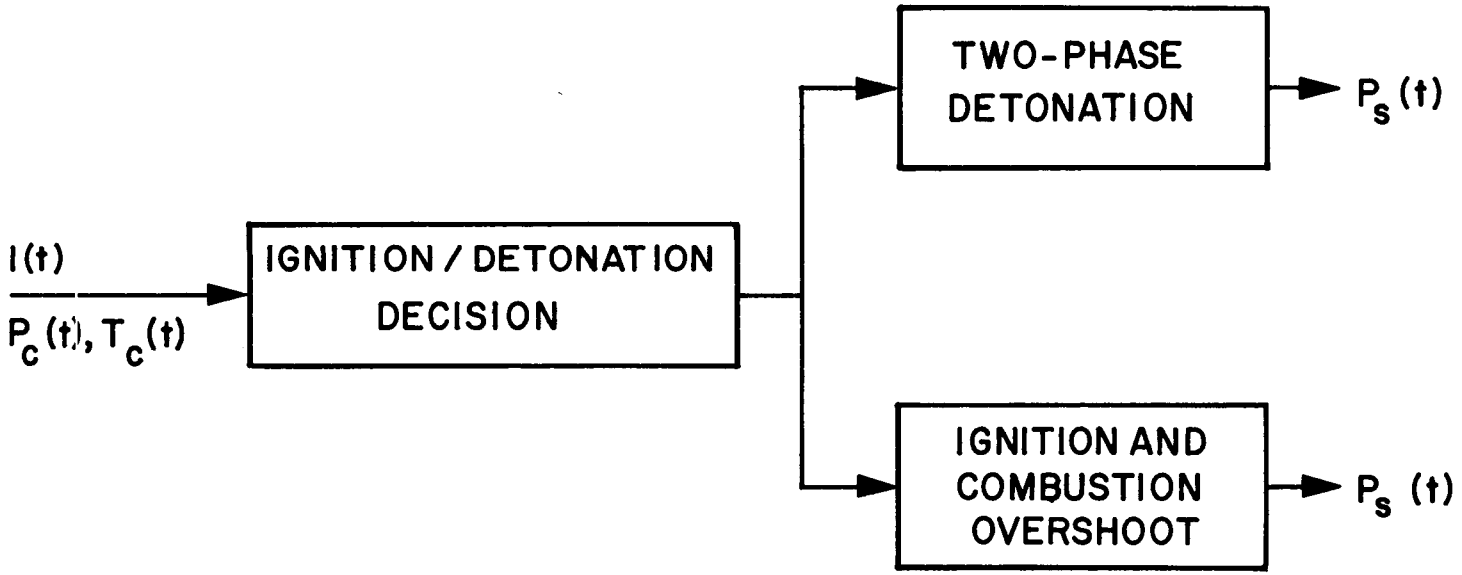

FIGURE 11. COMBUSTION/DETONATION SYSTEM (IV)

(3) The preignition chemistry and ignition delay (Figure 9), and

(4) The ignition process (Figure 10).

These four systems are described in this report along with a section on the chamber pressurization-ignition delay interrelationship.

In the transient flow system of Figure 7, the tank pressure is the input while the vapor, $V_1(t)$, and liquid, $L(t)$ flow rates into the chamber are the computed outputs.

The chamber pressurization system receives an input liquid flow at $L(t)$ and through the vaporization process shown in Figure 8, converts this liquid into vapor $V_2(t)$ and condensed phase material $C(t)$. The complete pressurization system must also account for initial vapor pressure flow through the injector orifice and preignition chemistry gas generation. The output of this system is the preignition chamber pressure $P_c(t)$, and temperature $T_c(t)$.

The preignition chemistry system of Figure 9 must be treated in greater detail than is available in the literature. Intermediate formation and gas generation contributes significantly to chamber pressurization. For example, with an oxidizer lead, high speed motion pictures indicate the presence of colorless N_2O_4 gas prior to fuel injection. However, almost instantaneously with fuel injection into the oxidizer vapor, redish brown NO_2 appears in the vapor space. This phenomenon may be due to heat generation or intermediate gas formation, either of which affect the chamber pressurization system of Figure 8. Thus the output of the preignition system will be the specification of intermediate vapor formation, $V_3(t)$, and intermediate products, $I(t)$, at $P_c(t)$ and $T_c(t)$.

The combustion/detonation system of Figure 11 involves an ignition or detonation decision based upon the incoming conditions of mixture, chamber pressure and temperature. This decision must be based upon propellant accumulation, heat loss, kinetics, and detonation transition length. Once the decision is made, the final spike produced, $P_s(t)$, or the combustion overshoot, $P_c(t)$, may be calculated by methods presented

in the order of magnitude calculations section.

The chamber ignition process is driven by a tank pressure signal, P_t, which passes through numerous complicated processes of varying importance and produces a detonation spike $P_s(t)$ or an ignition chamber pressure, $P_c(t)$.

Transient Flow. - The transient flow rate into the chamber must be known as a function of time in order to describe chamber pressurization.

The technique being applied involves analysis of experimental pressure-tap data and empirical specification of a lumped parameter system which is valid over a limited range of operating conditions.

Feed Line Dynamics. The range of conditions being treated at present are those encountered with pulse motor start-up at space-vacuum. The sketch below shows the diagrammatic setup.

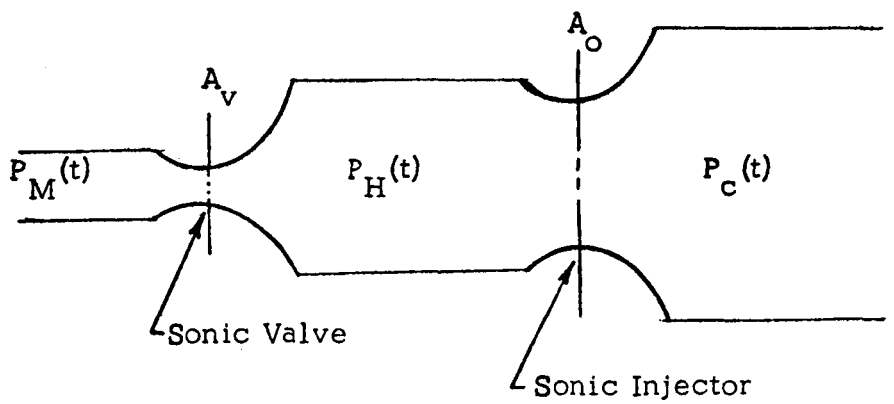

The tank pressure, $P_t(t)$, which may be assumed constant, is transmitted through the line impedance Z_L and results in the pressure $P_M(t)$, measured at the valve inlet and shown on the oscillograph trace below for the oxidizer $P_{MO}(t)$ and fuel $P_{MF}(t)$.

TYPICAL OSCILLOGRAPH TRACE

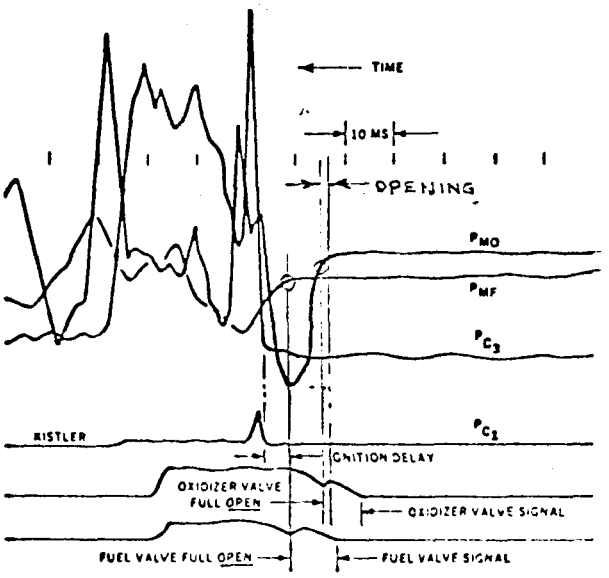

The valve opening time in this trace is approximately one millisecond while the inlet pressure P_{MO} continues to drop for approximately eight milliseconds.

The header pressure will equal the liquid vapor pressure previous to header filling. The time of header filling is determined from the volume of the header and the respective mass flow rates through the valve and injector. Once the header is filled, its pressure will rise to an equilibrium value.

By comparing both the header pressure and the chamber pressure with the vapor pressure, the appropriate mass flow equations can be applied. Thus, for the valve:

$$W = K\sqrt{P_M - P_V} \quad \text{for } P_H = P_V$$

$$W = K\sqrt{P_M - P_H} \quad \text{for } P_H > P_V$$

where:

P_V = vapor pressure

P_H = header pressure

K = a constant

For the injector:

$$W = \frac{P_H A^*}{\sqrt{T_M}} \sqrt{\frac{\gamma M}{R} \left(\frac{2}{\gamma+1}\right)^{\gamma+1/\gamma-1}} \qquad P_H = P_V \frac{P_C}{P_H} < \left(\frac{2}{\gamma+1}\right)^{\gamma/\gamma-1}$$

$$W = K\sqrt{P_H - P_V} \qquad P_H > P_V,\ P_C \leq P_V$$

$$W = K\sqrt{P_H - P_C} \qquad P_H > P_V,\ P_C > P_V$$

The pressure upstream of the manifold valve will be determined by a lumped parameter system while the flow rate into the chamber is determined by one of five sets of manifold/header/chamber pressure criteria. TRW recently had success in such a description by describing the feed line dynamics, on valve opening, with the following lumped parameter analog (Ref. 15).

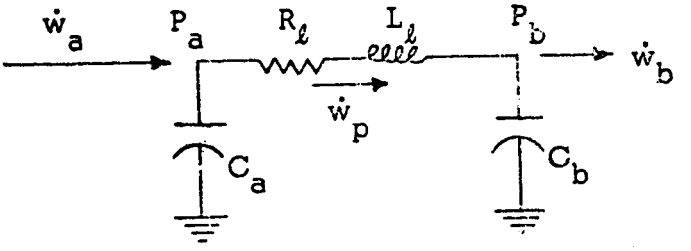

The equations describing flow in this system are derived for a mass balance:

$$C_a \frac{dP_a}{dt} = \dot{w}_a - \dot{w}_p$$

$$C_b \frac{dP_b}{dt} = \dot{w}_p - \dot{w}_b$$

and a momentum balance:

$$L \frac{d\dot{w}_p}{dt} = gA\,(P_a - P_b) - R\,(\dot{w}_p)^2$$

where:

$\dot{w}_a$ = section inlet flow rate, lb/sec

$\dot{w}_p$ = section instantaneous flow rate, lb/sec

$\dot{w}_b$ = section outlet flow rate, lb/sec

P_a = section inlet pressure, psia

P_b = section outlet pressure, psia

C = feed line capacitance, defined as

$$C = \frac{\rho AL}{144\beta}$$

C_a = effective feed line capacitance at station (a)

C_b = effective feed line capacitance at station (b)

β = propellant bulk modulus, lb/in.^{2}

$1/\beta$ = propellant compressibility, in.^{2}/lb, where

$$1/\beta_{MMH} = 3.20 \times 10^{-6} \text{ in.}^2/\text{lb}$$

$$1/\beta_{N_2O_4} = 5.31 \times 10^{-6} \text{ in.}^2/\text{lb}$$

ρ_{ox} = density of oxidizer = 90.31 lb/ft^3

ρ_F = density of fuel = 54.73 lb/ft^3

A = cross-sectional feed line flow area, in.^{2}

L = length of line per section, ft

g = acceleration due to gravity = 32.2 ft/sec^2

R = lumped feed line frictional loss coefficient, ft/lb

These three equations involve the input tank pressure P_a, and the four unknowns: Output manifold pressure P_b, and the three flow rates $\dot{w}_a$, $\dot{w}_p$, $\dot{w}_b$. The output flow rate $\dot{w}_b$ is related to the manifold pressure and the downstream header pressure by

$$P_b - P_H = R_v \left(\frac{\dot{w}_b}{A_v}\right)^2$$

where: $A_v(t)$ is the valve open area and is the driving force which actuates the system.

R_v is a variable nonlinear valve resistance for single and two-phase flow. The downstream pressure in the header determines the type of flow and resistance existing in the valve and injector orifice. It is found by accounting for the mass accumulation in the header by applying a series of flow regime criteria.

A slightly more complex computer program is being set up at the Manned Spacecraft Center in Houston (Ref. 16) which gives the flow rate into the chamber both with and without a preigniter. The model lumps feed line, injector, and combustor modules. The model was developed by both General Electric (Ref.17) and the Manned Spacecraft Center (Ref.16). Programming is nearing completion and this program could be used if desirable. However, this program does not treat two-phase and cavitating orifice flow, as is being attempted at Dynamic Science.

Cavitation. In order to determine the existence of two-phase flow the photographs of Figure 12 were recorded with a 10 microsecond flash unit for the N_2O_4/NO_2 flow system at the indicated time intervals after valve opening. The lighted portion of the first photograph shows a simulated two-dimensional manifold sandwiched between two pieces of plexiglass. In the next five photographs the N_2O_4/NO_2 vapor is the dark substance while the light penetrates through the liquid. Two-phase flow and cavitation are present during the entire filling sequence and even in the last photograph the injector orifice is fully cavitated. The transient flow equations are controlled during cavitating periods by the two phase flow resistance R_v. This proportionality constant will have to be determined experimentally as a function of back pressure and a digital program can then be written to solve the transient flow problem.

Chamber pressurization. - The following differential equations apply to the low pressure transient flow process when the liquid is at the same temperature as the vapor.

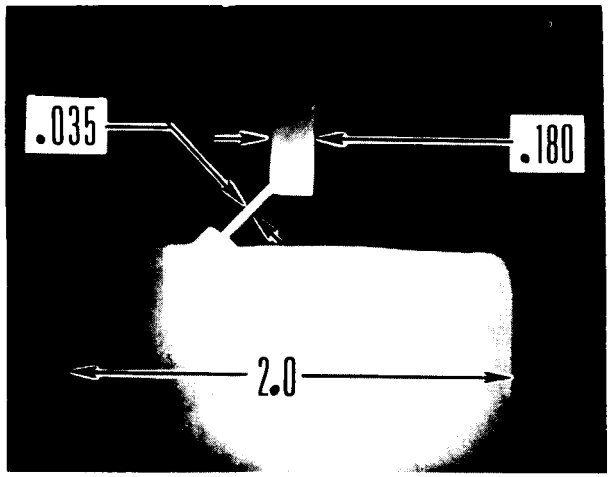

5 MILLISEC

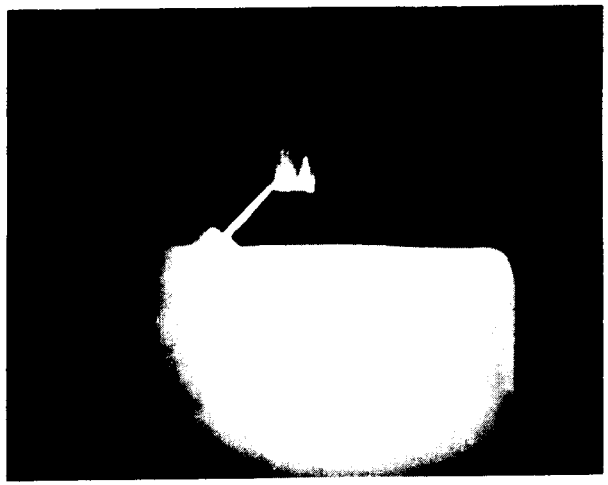

10 MILLISEC

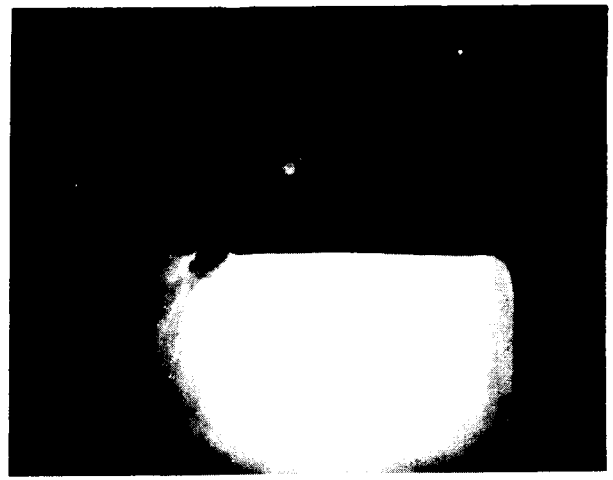

15 MILLISEC

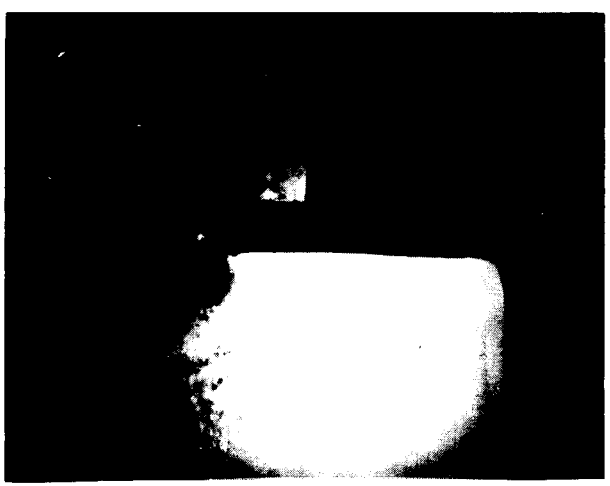

25 MILLISEC

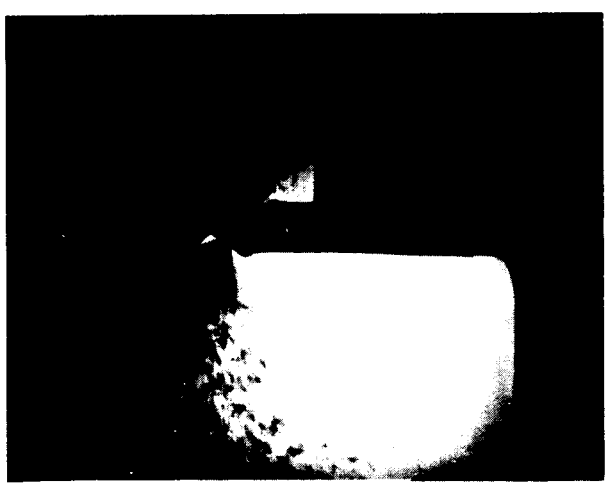

35 MILLISEC

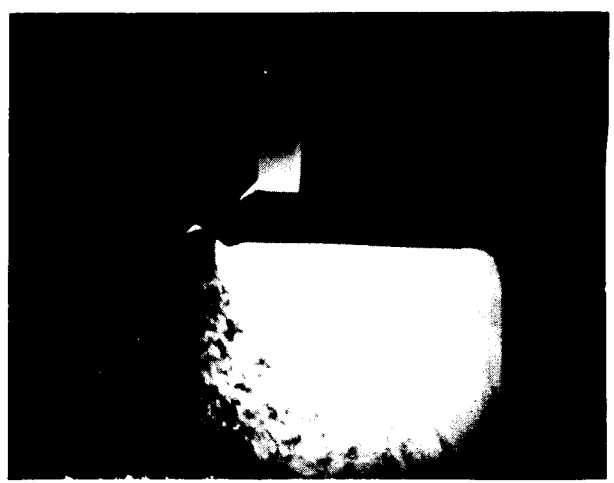

60 MILLISEC

FIGURE 12. N_2O_4 MANIFOLD FILLING SEQUENCE - $\dot{w}$ = .007 lb/sec, V = 10 ft/sec

$$\frac{dR}{dr} = \frac{100}{\sqrt{2\pi}\, r \ln\sigma} \exp\left[-\frac{1}{2}\left(\frac{\ln(r/\bar{r})}{\ln\sigma}\right)^2\right]$$

where:

R = per cent mass in drops smaller than given radius r

r = drop radius

σ = the geometric standard deviation

$\bar{r}$ = the mass median drop radius

Evaporation: $$\frac{dG_i}{dt} = \left[P_{VTd} - P_{gTg}\right] \alpha A_d \sqrt{\frac{Mg}{2\pi R T_d}}$$

where:

G_i = pounds mass of drop size i evaporated

t = time

P_{VTd} = vapor pressure evaluated at the temperature of the drop

P_{gTg} = gas pressure

α = accommodation coefficient

A_d = area of the drops

M = molecular weight

g = gravitational constant

R = universal gas constant

T_d = temperature of the drop

Condensation: $$\frac{dG_i}{dt} = \left[P_{gTg} - P_{VTw}\right] \alpha A_c \sqrt{\frac{Mg}{2\pi R T_g}}$$

where:

G_i = mass of drops of size i condensing

P_{VTw} = vapor pressure of the substance at the wall temperature

A_c = chamber wall area

T_g = gas temperature

Mass efflux out nozzle:

$$\frac{dm}{dt} = \frac{P_g A^*}{\sqrt{T_g}} \sqrt{\frac{\gamma M}{R} \left(\frac{2}{\gamma+1}\right)^{\gamma+1/\gamma-1}}$$

where:

m = mass flow out the nozzle

γ = ratio of heat capacities, C_p/C_v

A^* = the throat area

Heat balance on liquid drops:

$$\tau dG_i = \rho_\ell \frac{4}{3} \pi r_i^3 C_{p\ell} dT_i + \frac{4}{3} \pi \rho_\ell r_i^3 {}_{N-1} C_{ps} dT_{is}$$

where:

τ = heat of vaporization

G_i = pounds mass of drop size i evaporated

ρ_ℓ = liquid density

r_i = radius of the i^{th} drop group

$C_{p\ell}$ = heat capacity of liquid

T_i = temperature

C_{ps} = heat capacity of solid particles

T_{is} = temperature of i^{th} size solid drop

Since P_v, P_g, and T_d vary with time, it is necessary to use a numerical integration procedure. Agosta (Ref. 18) uses such a procedure:

Drop groups with specified mass distribution are determined from the logarithmiconormal distribution of Priem and Heidmann (Ref. 19).

Drop groups (i.e. n drop groups) with a given mass distribution are chosen. The number of drops N_i in each group is determined by

$$N_i = W_i / (r/3)\, \pi r^3 \rho_\ell$$

where: W_i = the mass of drops in each group.

Based on Knudson-Langmiur kinetic theory, it can be shown that the rate at which ideal gas molecules strike a surface is given by

$$G = P\sqrt{Mg/2\pi RT}$$

where:

G = mass of molecules striking a surface per unit area per unit time

P = gas pressure

R = gas constant

M = molecular weight

T = gas temperature

g = gravitational constant

If the surface is a liquid or solid condensate in equilibrium with its saturated vapor, and if the presence of the saturated vapor is denoted by P_v then the above equation becomes

$$G = P_v\sqrt{Mg/2\pi RT}$$

where: P_v = vapor pressure

If a fraction α of the molecules condenses on the surface, the equation becomes

$$G = \alpha P_v\sqrt{Mg/2\pi RT}$$

where: α = the accommodation coefficient

The equation gives the rate of evaporation from a surface in contact with its saturated vapor when both surface and vapor are at temperature T.

If some of the molecules that come off the condensate are not immediately removed so that a vapor cloud develops above the condensate surface, the net rate of evaporation is given by

$$G = \alpha(P_v - P_a)\sqrt{Mg/2\pi RT}$$

where: P_a = the pressure of the vapor cloud from a single drop. Thus the mass of liquid evaporating in a finite time interval is:

$$G_{ij} = \left[P_v(T_d)_{ij\ N-1} - P_g(T_g)_{N-1} \right] \alpha (r_{ij})^2_{N-1}\ \Delta t_n \sqrt{\frac{8\pi Mg}{R(T_d)_{ij\ N-1}}}$$

or

$$G_{ij} = C_i \left[P_v(T_d)_{ijN-1} - P_g(T_g)_{N-1} \right] \frac{\alpha r^2_{ijN-1} \sqrt{M}\ W_j\ \Delta t_N}{\rho_\ell \sqrt{(T_d)_{ijN-1}}}$$

where: C_i = a constant depending on the number of drops initially in an i^{th} group

$P_{v(T_d)_{ijN-1}}$ = the vapor pressure measured at the temperature of the i^{th} size drop of the j^{th} group at the end of the N-1 time interval.

$P_g(T_g)_{N-1}$ = gas pressure at the end of the N-1 time interval

r_{ij} = radius of the i^{th} size drop in the j^{th} group

Δt_N = time interval chosen

W_j = mass of liquid propellant injected during the j^{th} interval of time

$(T_d)_{ijN-1}$ = the temperature of the i^{th} size drop of the j^{th} group at the end of the N-1 time interval

j = drop groups, $1 \leq j \leq n$. j can start at a number greater than 1 if the initial drops become completely evaporated

The total evaporation occurring during the N^{th} time interval is:

$$(G_{EVAPN})_N = \sum_{i=1}^{n} \sum_{j=1}^{N} G_{ij}$$

At the end of every time interval, new drop radii and drop temperatures are calculated from:

$$G_{ij} = \frac{4}{3} \pi \rho_\ell \left[(r_{ij}^3)_{N-1} - (r_{ij}^3)_N \right]$$

and from the previous expression for G_{ij}

$$(r_{ij})_N = (r_{ij})_{N-1} \left[1 - \frac{K \left[P_v(T_d)_{ijN-1} - P_g(T_g)_{N-1} \right] \sqrt{M}\ \Delta t_N}{\rho_\ell\ r_{ijN-1} \sqrt{T_{dijN-1}}} \right]^{1/3}$$

where: K = a constant.

The new droplet temperatures are determined from a heat balance:

$$G_{ij}\tau = (4/3)\,\pi\rho_{\ell}\, r^{3}_{ijN-1} C_{p\ell}\,(T_{dijN-1} - T_{dijN})$$

and

$$T_{dijN} = T_{dijN-1} - \frac{K\tau\left[P_{v(T_d)_{ijN-1}} - P_{g(T_g)_{N-1}}\right]\sqrt{M\,\Delta t_N}}{\rho_{\ell}\, C_{p\ell}\, r_{ijN-1}\sqrt{T_{dijN-1}}}$$

If liquid freezing occurs, the term $x\ (4/3)\,\pi\,\rho_{\ell} r^{3}_{ijN-1}\,\tau$ fusion (where: x = the fraction of the liquid that has solidified) must be added to the right hand side of the heat balance equation.

If the liquid completely freezes and falls below the freezing temperature, the term:

$$(4/3)\,\pi\,\rho_{\ell} r^{3}_{ijN-1} C_{ps}(T_{sijN-1} - T_{sijN})$$

must also be added to the right hand side of the heat balance equation.

A separate $(G_{EVAPN})_N$ can be written for both the oxidizer and the fuel. The mass of vapor condensed on the chamber wall during the N^{th} time interval would be:

$$(G_{COND})_N = \left[P_{g(T_g)_{N-1}} - P_{v(T_s)}\right]\,\alpha A_c \Delta t_N \sqrt{\frac{Mg}{2\pi R(T_g)_{N-1}}}$$

Nozzle Flow: For isentropic flow of a perfect gas through a nozzle with constant values of C_p, M, and γ, the mass through the nozzle during the N^{th} time interval is:

$$(M_{NOZ})_N = \frac{P_{gN-1} A^*}{\sqrt{(T_g)_{N-1}}} \sqrt{\frac{\gamma Mg}{R}\left(\frac{2}{\gamma+1}\right)^{\gamma+1/\gamma-1}}\,\Delta t_N$$

A mass balance on the vapor gives at the end of the N^{th} time interval

$$(G_{EVAPN})_N - (G_{COND})_N - (M_{NOZ})_N = (M_c)_N - (M_c)_{N-1}$$

where:

$(M_c)_N$ = mass of vapor in the chamber at the end of the N^{th} time interval as determined from the ideal gas law

$= \frac{V_c M P_{gn}}{R T_{gN}}$, with V_c being the chamber volume.

$(M_c)_{N-1}$ = mass of vapor in the chamber at the end of the N-1 time interval $= \frac{V_c M}{R} \frac{P_{gN-1}}{T_{gN-1}}$

In order to determine P_{gN} from the mass balance equation for the vapor, Agosta (Ref.18) determines T_{gN} by means of a mass weighted average:

$$T_{gN} = \frac{\sum_{j=1}^{N} \sum_{i=1}^{n} G_{ij}(T_d)_{ijN-1} + (M_c)_{N-1} T_{gN-1} - (G_{COND})_N T_{gN-1} - (M_{NOZ}) T_{gN-1}}{\sum_{j=1}^{N} \sum_{i=1}^{n} G_{ij} + (M_c)_{N-1} - (G_{COND})_N - (M_{NOZ})_N}$$

Ignition delay and preignition chemistry. - In order to determine the conditions which exist in a rocket engine at and prior to ignition, it is necessary to know the ignition delay time and the preignition chemistry.

Knowing the pressure rise as a function of time, the ignition delay can be determined from a knowledge of the variation of ignition delay with ambient pressure. This information can be determined experimentally and in some cases is known.

Reaction Motors Division (Ref. 7) has experimental data for the system N_2O_4-UDMH which fits the equation

$$\ell n\, \tau_D = 15.5 - 2.6\, \ell n\, (Pa)$$

where

τ_D = ignition delay

Pa = ambient pressure

Although this particular correlation applies only to N_2O_4-UDMH, experimental

data of ignition delay versus ambient pressure is available for N_2O_4-A50, N_2O_4-MMH and IRFNA-UDMH.

A theoretical determination of the ignition delay can be based on the criterion that ignition occurs when the heat generated just exceeds the heat loss. This criterion is true for thermal ignition mechanisms, i.e., no chain branching, and is probably true for hypergolic propellant systems.

The rate of heat generation in a rocket engine can be expressed by:

$$q_g = \Delta HVr + h_{wl} A_w (T_w - T)$$

where

ΔH	=	the heat of reaction
V	=	volume of thrust chamber
r	=	Arrhenius reaction rate
h_{wl}	=	heat of transfer coefficient from the chamber wall to the propellants
A_w	=	chamber wall area
T_w	=	wall temperature
T	=	propellant temperature

The reaction rate is determined from:

$$r = K C_o^n C_F^m d^{-E/RT}$$

where:

K	=	a constant
C_o	=	oxidizer concentration
C_F	=	fuel concentration
n and m	=	experimentally determined exponents
E	=	activation energy

The heat loss can be determined from:

$$q_{loss} = (hA + WC_p)(T - T_o) + h_{w2} A_w (T - T_w)$$

where :

h	= heat transfer coefficient between gas in the thrust chamber and liquid and solid particles
A	= combined area of the liquid and solid particles
W	= flow rate out the nozzle
C_p	= specific heat of reactant mixture
T	= propellant temperature
T_o	= temperature of incoming propellant
h_{w2}	= heat transfer coefficient from propellant to wall
A_w	= chamber wall area
T_w	= wall temperature

The rate of change of temperature with time, based on an energy balance is,

$$\frac{dT}{dt} = \frac{\Delta H K C_o^n C_F^m e^{-E/RT}}{\rho C_p} + \frac{h_{w1} A_w (T_w - T)}{m C_p} - \frac{(hA + WC_p)(T - T_o)}{m C_p} - \frac{h_{w2} A_w (T - T_w)}{m C_p}$$

where: m = the mass of the system

ρ = density of the system

That portion of the heat generation term that deals with preignition chemistry (in this case N_2O_4-N_2H_4) was examined analytically with a preliminary kinetic model.

The reaction rate of the low pressure, N_2O_4-N_2H_4 gas reaction was determined from the collision theory which states that:

$$r = K C_A C_B$$

$$K = A e^{-E/RT}$$

$$A = \sigma_{AB}^2 \left(8\pi RT \frac{M_A + M_B}{M_A M_B}\right)^{1/2}$$

where K = reaction rate constant, cc/(molecule)(sec.)

$C_A = C_{N_2O_4}$ = concentration of nitrogen tetroxide, molecules/cc

C_B = $C_{N_2H_4}$ = concentration of hydrazine, molecules/cc

A = frequency factor

E = activation energy

σ_{AB} = effective diameter of A and B upon collision

$= \frac{\sigma_A + \sigma_B}{2}$

M_A, M_B = molecular weights

R = gas constant = $K_B N_A$, the product of Boltzmann's constant and Avogadro's number, ergs/(^oK)(g mole)

In this analysis a one to one molar ratio of reactants is assumed along with a reaction which is first order with respect to each reactant.

For use in the equation, the collision diameters were calculated from the cube root of the respective molecular volumes. The molecular volumes of nitrogen tetroxide and hydrazine were determined from the sum of the respective atomic volumes (Ref. 20). Thus,

$$\sigma_{N_2H_4} = 4.25 \times 10^{-8} \text{ cm} = 4.25\text{Å}$$

$$\sigma_{N_2O_4} = 4.7 \times 10^{-8} \text{ cm} = 4.7\text{Å}$$

The activation energy, E, for the reaction was determined from one fourth the sum of the bond energies broken. In this case the sum of the bond energies broken is determined by postulating a reaction initiated by the following decomposition reactions:

$$N_2O_4(g) \rightarrow N_2 + 2O_2 \qquad \Delta H_{298.15^oK} = -2.35 \text{ Kcal/mole}$$

$$3N_2H_4(g) \rightarrow 4NH_3 + N_2 \qquad \Delta H_{298.15^oK} = -37 \text{ Kcal/mole}$$

Liquid hydrazine thermally decomposes to NH_3 and N_2 at high temperatures in very short time intervals, such as transient times in

rocket engines (Ref. 21). The same decomposition reaction is assumed to hold for gaseous hydrazine. The activation energy is taken as one fourth the sum of the respective heats of dissociation of the above reactions, thus E= 9.84 Kcal/mole.

Substituting in the above expression for reaction rate, one obtains:

$$r = \left[\frac{4.25\times10^{-8}+4.7\times10^{-8}}{2}\right]\left[8(3.14)(8.3)(10^{7})\frac{92+32}{92(32)}\right]^{1/2} e^{\frac{-9840}{1.98T}} C_{N_2O_4}$$

$$\times C_{N_2H_4} \frac{\text{Molecules}}{\text{cc(sec)}}, \text{ or}$$

$$r = 1.128T^{1/2}\ 10^{10} e^{-4969.7/T}\ C_{N_2O_4} C_{N_2H_4} \frac{\text{moles}}{\text{liter(sec)}}$$

If complete equilibrium reaction of $N_2O_4 + N_2H_4$ takes place, water and nitrogen are formed as products:

$$N_2O_4 + 2N_2H_4 \rightarrow 4H_2O + 3N_2.$$

The heat of reaction for liquid nitrogen tetroxide with liquid hydrazine is -248 Kcal/mole. However, experiments at Dynamic Science have shown that for liquid nitrogen tetroxide and liquid hydrazine reacting at room temperature, the heat of reaction is of the order of 30Kcal/mole. Assuming this same heat of reaction for a gaseous reaction at room temperature, the rate of temperature change becomes:

$$\frac{dT}{dt} = \frac{(30)\ 1.128T^{1/2}10^{10} C_{N_2O_4} C_{N_2H_4} e^{-4969.7/T}}{\rho C_p}$$

Chamber Pressurization - Ignition Delay Interrelationship:

The mass weighted average temperature

$$T_{gN} = \frac{\sum_{j=1}^{N} \sum_{i=1}^{n} G_{ij} (T_d)_{ijN-1} + (M_c)_{N-1}(T_g)_{N-1} - (G_{COND})_N (T_g)_{N-1} - M_{NOZ}(T_g)_{N-1}}{\sum_{j=1}^{N} \sum_{i=1}^{n} G_{ij} + (M_c)_{N-1} - (G_{COND})_N - (M_{NOZ})_N}$$

takes into account the change in gas temperature due to evaporation, condensation, and gas efflux from the nozzle.

In this analysis, the gas temperature will be determined from:

$$T_{gN} = \frac{\sum_{j=1}^{N} \sum_{i=1}^{n} G_{ij} (T_d)_{ijN-1} + (T_g)_{N-1}(M_c)_{N-1} - (G_{COND})_N (T_g)_{N-1} - (M_{NOZ})_N (T_g)_{N-1} - (M_s)_N (T_g)_{N-1}}{\sum_{j=1}^{N} \sum_{i=1}^{n} G_{ij} + (M_c)_{N-1} - (G_{COND})_N - (M_{NOZ})_N - (M_s)_N}$$

$$+ \frac{\Delta H K C_o^n C_F^m e^{-E/R(T_g)_{N-1}}}{\rho C_p} \Delta t_N + \frac{h_{w1} A_w (T_w - T)}{m C_p} \Delta t_N$$

$$- \frac{(hA + WC_p)(T - T_o)}{m C_p} \Delta t_N - \frac{h_{w2} A_w (T - T_w)}{m C_p} \Delta t_N$$

where $(M_s)_N$ = mass of solid or liquid intermediate compound formed during the N^{th} time interval.

Pressurization as a function of time will then include the effects of evaporation, condensation, mass flow out the nozzle, intermediate compound formation, gaseous chemical reaction, and heat transfer to and from the wall.

The pressurization equation then becomes:

$$\sum_{i=1}^{N} \sum_{j=1}^{n} C_i \left[P_v (T_d)_{ijN-1} - P_g (T_g)_{N-1} \right] - \frac{\alpha r^2_{ijN-1} \sqrt{M} \; W_j \Delta t_N}{\rho_\ell \sqrt{(T_d)_{ijN-1}}}$$

$$- \left[P_{g(T_g)_{N-1}} - P_{v(T_s)} \right] \alpha A_c \Delta t_N \sqrt{\frac{Mg}{2\pi R(T_g)_{N-1}}}$$

$$- \frac{(P_g)_{N-1} A^*}{\sqrt{(T_g)_{N-1}}} \sqrt{\frac{\gamma M}{R}} \left(\frac{2}{\gamma+1} \right)^{\frac{\gamma+1}{\gamma-1}} \Delta t_N - (M_s)_N \Delta t_N = \frac{V_c M}{R} \left[\frac{P_{gN}}{T_{gN}} - \frac{P_{gN-1}}{T_{gN-1}} \right]$$

Ignition process. - The transient model being developed will determine the conditions in the chamber at all times up to ignition.

The pressure generated by either a detonation or an explosion can be calculated. The equation $P_2/P_1 = (1+\alpha\gamma_1 M_1^2)/1+\gamma_2$ can be applied to determine the magnitude of the transient overpressure due to a detonation. The use of this equation will depend upon whether the detonation induction distance and engine contraction ratio (A_c/A_t) criteria are satisfied.

The magnitude of a transient overpressure due to an explosion can be calculated from the ideal gas law. This can be done by assuming that the propellants react instantaneously throughout the entire chamber volume or that they collect and react in only a small segment of the chamber.

Mathematically, this problem area has been reasonably solved. The magnitude of the detonation or explosion can be determined from conditions existing at ignition. The identification of the triggering mechanism will probably have to be determined experimentally. However, studies can be made of different spiking mechanisms (such as formation of hydrazinium nitrate, explosion or reaction of frozen propellants on the chamber wall, etc.), so as to help design an engine minimizing the occurrence of excessive initiating transient overpressure.

Results of Chamber Pressurization Computations

By means of the chamber pressurization program, the gas pressure, gas temperature, mass of propellant evaporated, mass of gas condensed, mass efflux from the nozzle, liquid drop temperature, and fraction of a liquid drop frozen can be computed for the nitrogen tetroxide-Aerozine 50 system. The applicable computer program listing is given in Appendix A. In its present state, the pressurization program treats each propellant separately, that is, pre-ignition chemical kinetics, the related chemical energy release and temperature change have not been incorporated in the computer code to date. However, these interaction effects have been formulated analytically. It should be emphasized that the chemical kinetic parameters for the important hypergolic propellant reactions are difficult to determine, but that meaningful parametric studies can be performed within the framework of the analytical model.

Parametric studies. - Several parametric studies, the results of which are given graphically in Figures 13 through 16, were carried out utilizing the present pressurization program. In these studies, the dependence of the chamber pressure on the flow rate, chamber wall temperature, accommodation coefficient, and droplet radius is determined.

Figure 13 shows the variations of chamber pressure history with flow rate for the oxidizer (N_2O_4) and fuel (Aerozine-50) separately. A 40 percent increase in flow rate from 0.345 lb/sec to 0.483 lb/sec brings about a maximum absolute increase in chamber pressure of $\approx$0.33 psia for the oxidizer at $\approx$2.3 msec after injection. In the case of the fuel, the same change in flow rate yields an increase in chamber pressure of $\approx$0.13 psia which does not vary with time after $\approx$2 msec.

The calculations of the effect of wall temperature on chamber pressure (Figure 14) show that for N_2O_4 during the first msec, a relatively small difference in pressurization rate is obtained, whereas after $\approx$4 msec at least at 1 psia difference in chamber pressure is obtained for a 91°F change in wall

temperature.

Figure 15 shows the significant effect of the accommodation coefficient on early pressurization rate and on the absolute pressure values obtained after a few msec following injection. This figure applies to N_2O_4 and is based on an initial droplet temperature of $530^{\circ}R$.

The effect of oxidizer droplet radius on chamber pressurization is demonstrated in Figure 16. As one would expect, smaller drop radii enhance chamber pressurization. Since the oxidizer flow rate is only 1/4 of the highest value employed in the calculations, both sets of droplet radii, even after 7 msec, yield a comparatively low chamber pressure, that is, below 1.5 psia.

The above computational studies have demonstrated the relative effect of several important parameters governing the physical processes taking place within the combustion chamber. Further development of the mathematical model will make possible the quantitative study of additional chemical and physical interactions, and thus help to define engine design and operating conditions minimizing or eliminating spiking.

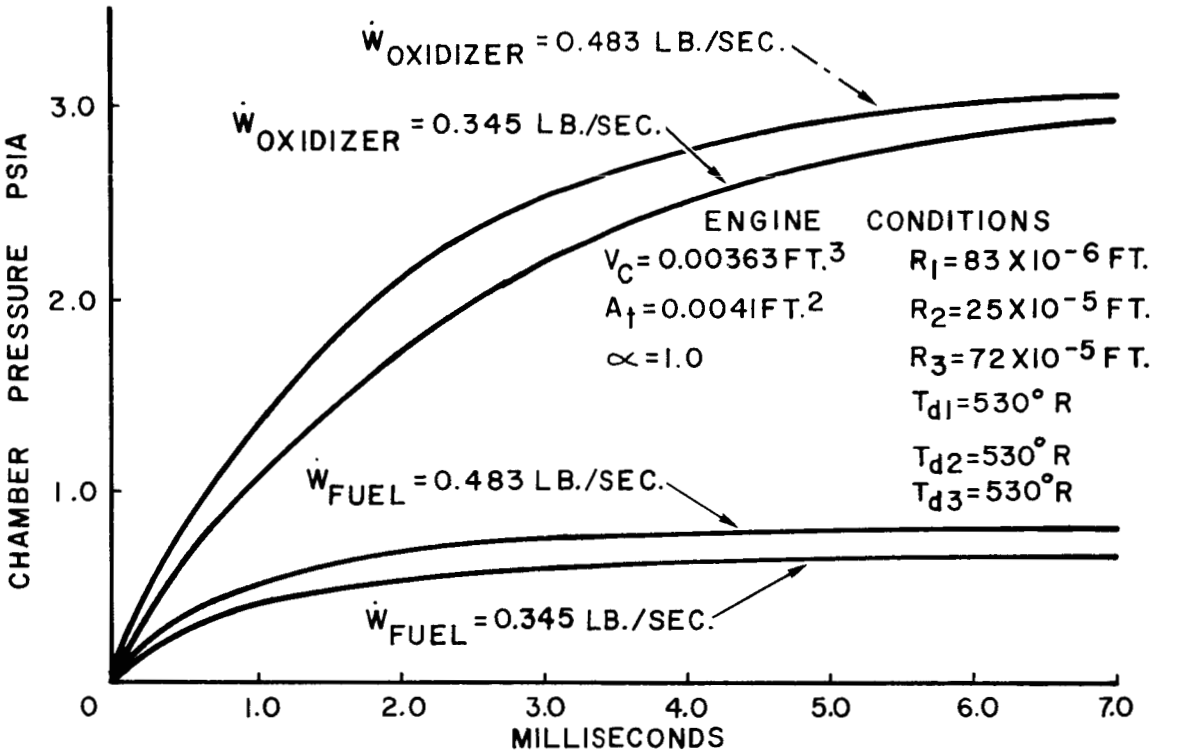

FIGURE 13. EFFECT OF FLOW RATE ON PRESSURIZATION.

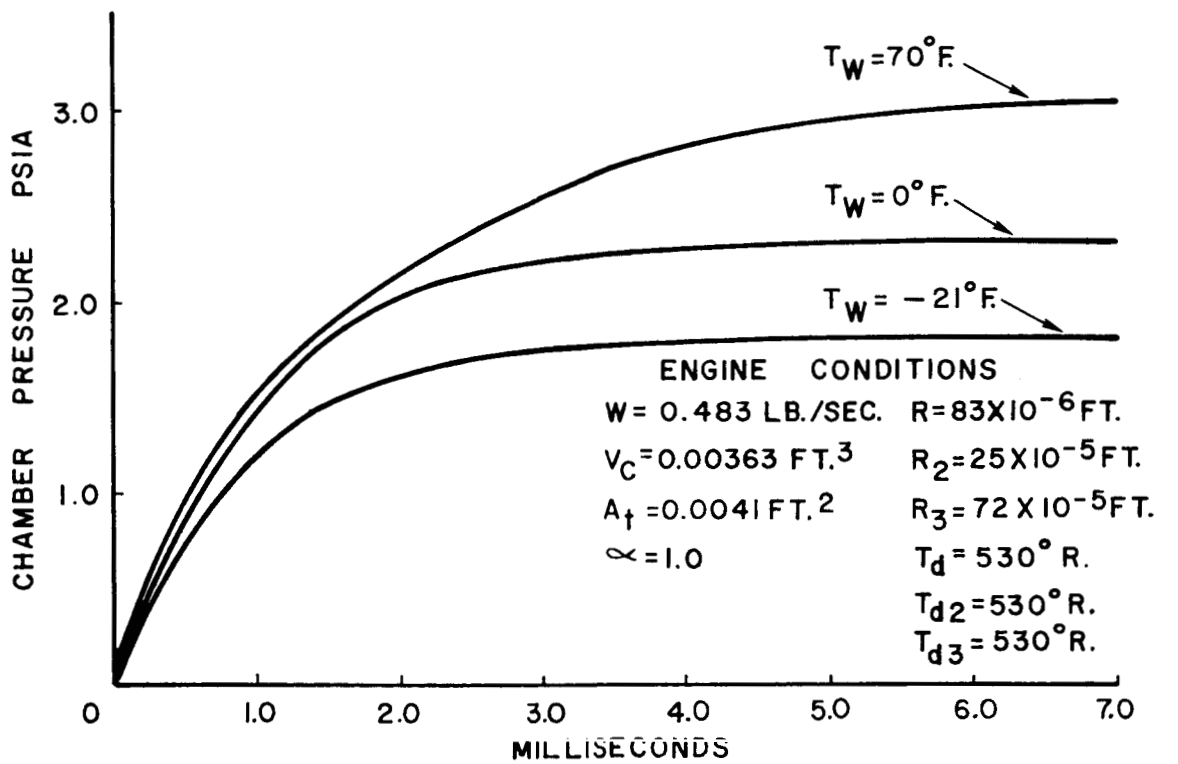

FIGURE 14. EFFECT OF WALL TEMPERATURE ON OXIDIZER PRESSURIZATION.

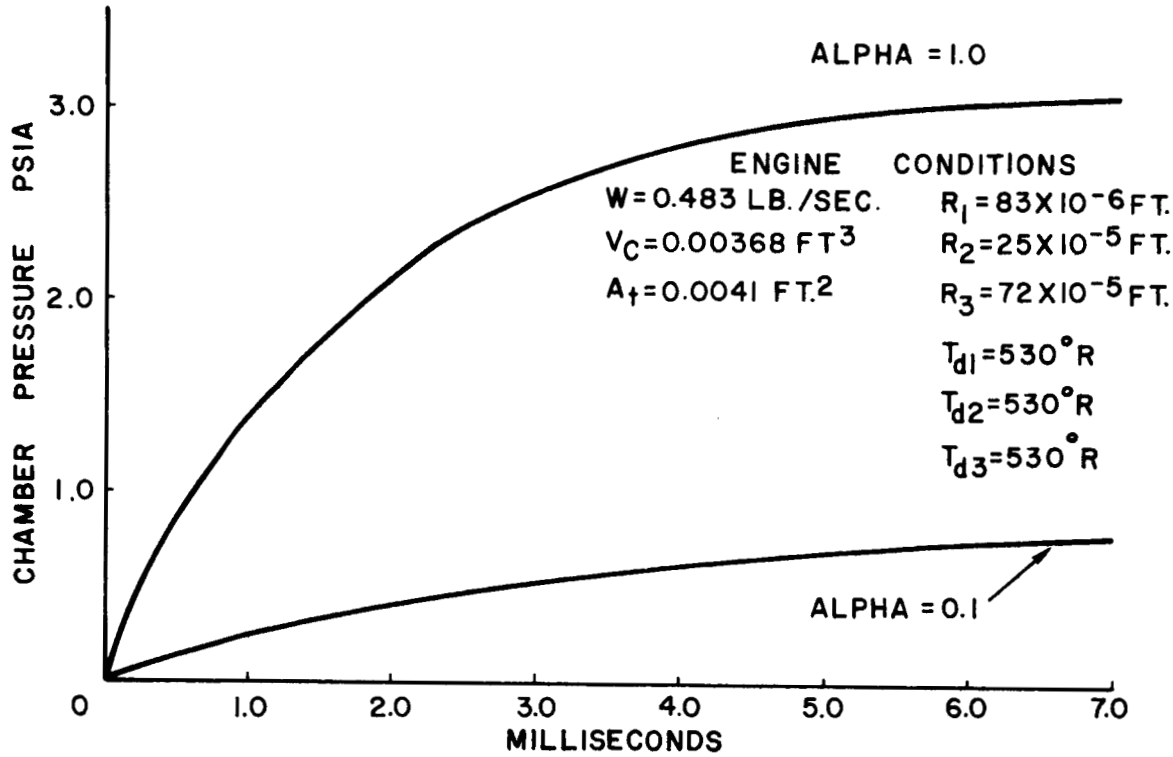

FIGURE 15. EFFECT OF ACCOMMODATION COEFFICIENT ON OXIDIZER PRESSURIZATION.

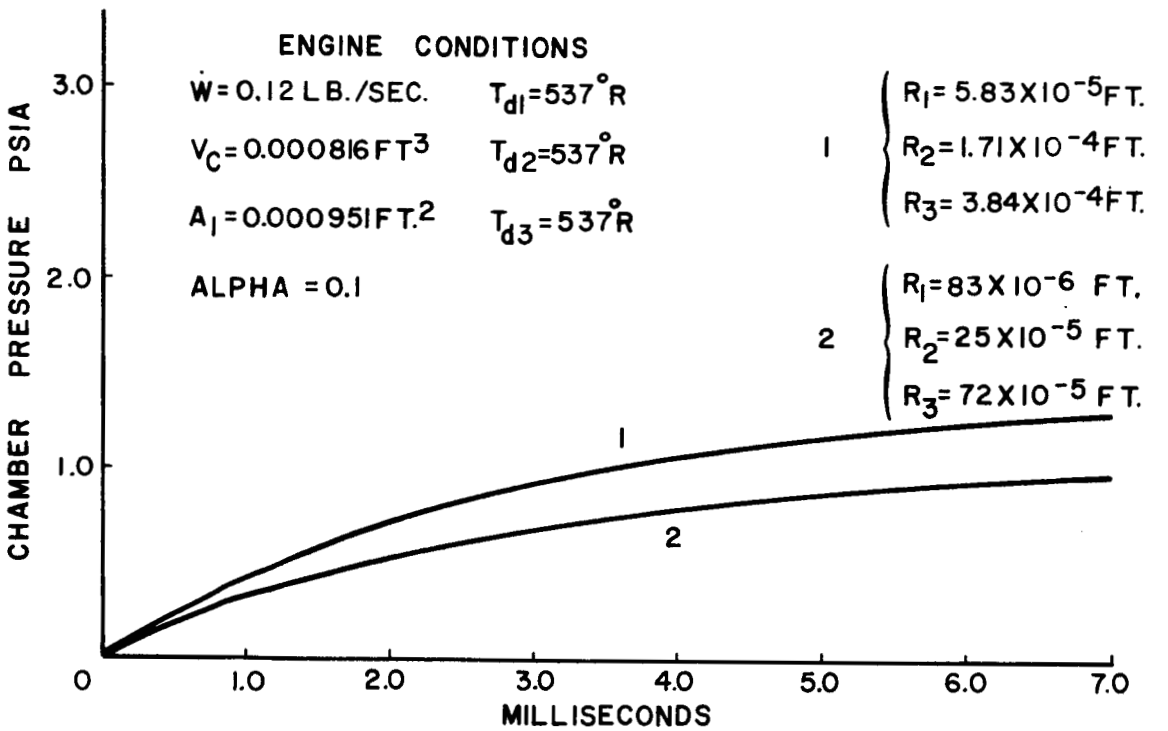

FIGURE 16. EFFECT OF DROPLET RADIUS ON OXIDIZER PRESSURIZATION.

VI. CONCLUSIONS

The following enumeration presents significant conclusions which were drawn from the experimental, order of magnitude, literature survey, and computational work concerning overpressure phenomena carried out in this study:

(1) Experiments showed that cavitation and two-phase flow is present within the injector during the space starting sequence of an engine, and that this phenomenon may significantly limit the initial flow rates.

(2) It was shown that especially in regions close to the injector face high amplitude detonation waves can be supported by a two-phase propellant mixture, whereas one-phase, gaseous detonation produces relatively low detonation pressures anywhere in the chamber. Thus, in the nitrogen tetroxide-hydrazine system observed high amplitude overpressures may only be accounted for by two-phase detonations.

(3) Heterogeneous detonation calculations show order of magnitude agreement with maximum spike pressures observed in certain engines.

(4) Existing literature indicates that intermediate reaction products (gaseous, liquid, and solid) may play an important role in spiking.

(5) It is not clear whether transient overpressures stem from material (intermediates or pure propellants) accumumulated on the walls or originate from reactions in the combustion chamber space. This points to the importance of understanding the triggering mechanism.

(6) The mathematical model developed in this study, in its present state, is capable of predicting chamber conditions during the preignition time period. The computer solution may be used to perform parametric design studies.

REFERENCES

1. Knox, R. M.; Minton, S. J.; and Zwick, E. B.: Space Ignition. Paper presented at AIAA Second Propulsion Joint Specialist Conference (Colorado Springs, Colorado), June 13-17, 1966.

2. Minton, S. J.; and Zwick, E. B.: Hypergolic Combustion Initiated at Low Pressure. Paper presented at the Aviation Space Conference of the American Society of Mechanical Engineers, (Los Angeles, California), March 16, 1965.

3. Kappl, J. J.; and Knox, R. M.: Altitude Ignition of Hypergolic Bipropellant Rockets. The Marquardt Corporation.

4. Bernard, J. L. J.; and Dufour, J.: Eigth International Symposium on Combustion. On the Existence of Detonation Conditions in the Combustion of Some Nitric Acid Propellants. 1960, pp. 1074-1084.

5. Martens, R. E.: Investigation of the Hypergolic Ignition Spike Phenomena. Internal Report, Engineering Technology Division, McDonnel Aircraft Corporation.

6. Chaffee, Norman H.; NASA Manned Spacecraft Center, (Houston, Texas) Verbal Communication.

7. Thiokol Chemical Corporation, Reaction Motors Division: Hypergolic Ignition at Reduced Pressures. AFRPL-TR-64-175, December 1964.

8. Lawver, B. R.; and Kappl, J. J.: Effects of Additives on Altitude Hypergolic Ignition. Paper presented at AIAA Second Propulsion Joint Specialist Conference (Colorado Springs, Colorado), June 13-17, 1966.

9. Lawver, B. R.: Effect of Ignition O/F on Spike Pressure Distribution. Interoffice Memo 153-75/49, Marquardt Corporation, May 1966.

10. Skinner, B. G.; Hedley, W. H.; and Snyder, A. D.: Mechanism and Chemical Inhibition of the Hydrazine-Nitrogen Tetroxide Reaction. (ASD-TDR-62-1041), Monsanto Research Corporation, December 1962.

11. Weiss, H. G.: A Basic Study of the Nitrogen Tetroxide-Hydrazine Reaction. (Contract No. NAS7-100), Dynamic Science, July 1965.

12. Friedman, R.; Barnes, W. P.; and Markels, M. Jr.: A Study of Explosions Induced by Contact of Hydrazine-Type Fuels with Nitrogen Tetroxide. Technical Documentary Report (ASD-TR-62-685), Atlantic Research

Corporation, September, 1962.

13. Perlee, Henry E.; and Christos, Theodore: Summary of Hypergolic Ignition Spike Phenomena. U. S. Department of the Interior, Bureau of Mines Final Report No. 3982, April 8 to December 31, 1965.

14. Ragland, K. W.; Dabora, E. K.; and Nicholls, J. A.: Shock Induced Heterogeneous Detonations. [Preprint]WSCI 65-22, Fall Meeting of Western States Section, The Combustion Institute, October 1965.

15. Kliegel, J. R.; et. al.: C-1 Engine Final Report. TRW Systems, 5380-6005-RU000, September 3, 1965.

16. Martinez, E. P.: Propellant Feed System Hydraulics in L/M Reaction Control System. Propulsion and Power Division, Manned Spacecraft Center. (Houston, Texas), 1966.

17. Bowling, R. C.; and Rope, R. K.: Dynamic Interaction Analysis and Computer Model LM Reaction Control Propulsion System. Advanced Technology Laboratories, General Electric Company, March 1965.

18. Agosta, Vito D.; and Graus, George: An Investigation of the Impulse Bit Developed by a Pulsed Liquid Propellant Rocket Engine. Curtiss-Wright Corporation.

19. Priem, R. J.; and Heidmann, M. F.: Propellant Vaporization as a Design Criterion for Rocket-Engine Combustion Chambers. NASA TR-67, 1960.

20. Perry, J. H.: Chemical Engineers Handbook. Third ed., 1950, p. 538.

21. Thomas, D. D.: The Thermal Decomposition of Hydrazine. Progress Report No. 9-14, Jet Propulsion Laboratory, August 6, 1947.

22. Weiss, Richard R.; and Klopotek, Raymond D.: Experimental Evaluation of the Titan III Transtage Engine Combustion Stability Characteristics. (AFRPL-TR-66-51), March 1966.

23. Weiss, R. R.; Chew, T. J.; and Klopotek, R. D. Lt.: A Combustion Stability Evaluation of Various Hydrazine and Hydrazine Blend Fuels. Air Force Rocket Propulsion Laboratory.

24. Clayton, R. M.: Combustion Roughness and Dynamic Stability. Jet Propulsion Laboratory, (a section of a future report).

DISTRIBUTION LIST

Chief, Liquid Propulsion Experimental Systems, RPX
NASA
Washington, D. C. 20546 (4)*

Chief, Liquid Propulsion Technology, RPL
NASA
Washington, D. C. 20546 (4)

Director, Launch Venicles and Propulsion, SV
NASA
Washington, D C. 20546

Director, Advanced Manned Missions
MT - NASA
Washington, D. C. 20546

Director, Mission Analysis Division
NASA Ames Research Center
Moffett Field, Calif. 24035

Air Force Rocket Propulsion Laboratory
Research and Technology Div. (2)
Air Force System Command
Edwards, California 93523
Mr. S. R. Bornhorst
Lt. G. J. Abbe

U.S.Naval Ordnance Test Station
China Lake, Calif. 93553
Mr. E. Price

Jet Propulsion Laboratory (3)
4800 Oak Grove Drive
Pasadena, Calif. 91103
Mr. R. M. Clayton
Dr. R. Kushida
Mr. J. H. Rupe

NASA Pasadena Office (2)
4800 Oak Grove Drive
Pasadena, California 91103
Contracting Officer
Office of Technical Information & Patent Matters

Scientific and Technical Information Facility (25)
Attn: NASA Representative, Code CRT
P.O.Box 5700
Bethesda, Maryland 20014

Lewis Research Center (4)
21000 Brookpark Road
Cleveland, Ohio, 44135
Mr. E. W. Conrad
Dr. C. Feiler
Dr. R. J. Priem
Marshall C. Burrows

Marshall Space Flight Center
Huntsville, Alabama, 35812 (2)
Mr. Kieth Chandler
Mr. R. Richmond

Manned Spacecraft Center
Houston, Texas 77001
Mr. J. G. Thibodaux

NASA Field Centers

Ames Research Center (2)
Moffett Field, Calif. 94035
Harold Hornby
Clarence A. Syvertson, Mission Analysis Division

Goddard Space Flight Center (2)
Greenbelt, Maryland 20771
Merland L. Moseson, Code 620
Mr. D. Grant

Jet Propulsion Laboratory
California Institute of Technology (2)
4800 Oak Grove Drive
Pasadena, Calif. 91103
Henry Burlage Jr.
Propulsion Div., 38

Langley Research Center (2)
Langley Station
Hampton, Virginia 23365
Dr. Floyd L. Thompson, Director
Mr. R. Hook

*Indicates number of copies.

Lewis Research Center (2)
21000 Brookpark Road
Cleveland, Ohio 44135
Dr. Abe Silverstein, Director
Mr. I. A. Johnsen

Marshall Space Flight Center (2)
Huntsville, Alabama 35812
Hans G. Paul, Code R-P+VED
Werner Voss, R-P and VE-PM

Manned Spacecraft Center (2)
Houston, Texas 77001
Dr. Robert R. Gilruth, Director
Mr. H. Pohl

Western Support Office (2)
150 Pico Boulevard
Santa Monica, Calif. 90406
Robert W. Kamm, Director

John F. Kennedy Space Center, NASA (2)
Cocia Beach, Florida 32931
Dr. Kurt H. Debus

NASA Test Facility
Propulsion Engineering Office
White Sands, New Mexico
I.D.Smith, Staff Chemist

Government Installations

Aeronautical Systems Division
Air Force Systems Command
Wright-Patterson Air Force Base
Dayton, Ohio 45433
D. L. Schmidt
Code ASRCNC-2

Air Force Missile Development Center
Holloman Air Force Base
New Mexico, 88330
Maj. R. E. Bracken
Code MDGRT

Air Force Missile Test Center
Patrick Air Force Base, Florida
L. J. Ullian

Air Force Systems Division
Air Force Unit Post Office
Los Angeles, Calif. 90045
Col. Clark, Technical Data Center

Technical Library (2)
AFFTC(FTBPP-2)
Edwards AFB Calif. 93523
Myrtle C. Jones

Arnold Engineering Development Center
Arnold Air Force Station
Tullahoma, Tennessee 37388
Dr. H. K. Doetsch

Bureau of Naval Weapons
Department of the Navy
Washington, D.C. 20546
J. Kay, RTMS-41

Defense Documentation Center
Headquarters
Cameron Station, Building 5
5010 Duke Street
Alexandria, Virginia 22314
Attn: TISIA

Headquarters, U.S. Air Force
Washington 25, D.C. 20546
Col. C.K.Stambaugh, AFRST

Picatinny Arsenal
Dover, New Jersey 07801
I. Forsten, Chief, Liquid Propulsion
Laboratory, SMUPA-DL

Air Force Office of Scientific
Research (OAR)
Arlington, Virginia 22209
Dr. B. T. Wolfson

Air Force Rocket Propulsion Laboratory
Research and Technology Division (2)
Air Force Systems Command
Edwards, California 93523
RPRR/Mr. H. Main
1/Lt. D. Shantz

U.S. Atomic Energy Commission
Technical Information Services
Box 62
Oak Ridge, Tennessee 37830
A. P. Huber
Oak Ridge Gaseous Diffusion Plant
(ORGDP) P.O. Box P

U.S. Army Missile Command
Redstone Arsenal
Alabama 35809
Dr. Walter Wharton

U.S. Naval Ordnance Test Station
China Lake, Calif. 93557
Code 4562, Chief, Missile
Propulsion Division

CPIA

Chemical Propulsion Information
Agency
Applied Physics Laboratory
8621 Georgia Avenue
Silver Spring, Maryland 20910
Mr. P. Martin

Industry Contractors

Aerojet-General Corporation
P.O. Box 296
Azusa, California 91703
Mr. L. F. Kohrs

Aerojet-General Corporation
P.O. Box 1947
Technical Library, Bldg. 2015, Dept. 2410
Sacramento, California 95809
Mr. R. Stiff

Aeronutronic Division
Philco Corporation
Ford Road
Newport Beach, Calif. 92663
Mr. N. Stern

Aerospace Corporation (2)
2400 East El Segundo Boulevard
P.O. Box 95085
Los Angeles, Calif. 90045
Mr. M. J. Russi
Mr. H. Greer, Propulsion Department

Technical Library
Air Research Mfg. Co.
9851 Sepulveda Blvd.
Los Angeles, Calif. 90045
Mr. C. S. Coe

Arthur D. Little, Inc.
20 Acorn Park
Cambridge, Massachusetts 02140
E. Karl Bastress

Astropower Laboratory
Douglas Aircraft Company
2121 Paularino
Newport Beach, Calif. 92663
Dr. George Moc, Director, Research

Astrosystems International, Inc.
1275 Bloomfield Avenue
Fairfield, New Jersey 07007
Mr. A. Mendenhall

Atlantic Research Corporation
Edsall Road and Shirley Highway
Alexandria, Virginia 22314
Mr. A. Scurlock

Beach Aircraft Corporation
Boulder Division
Box 631
Boulder, Colorado 80302
Mr. J. H. Rodgers

Bell Aerosystems Company (2)
P.O. Box 1
Buffalo, New York 14240
Mr. N. R. Roth
Mr. J. Flanagan

Bendix Systems Division
Bendix Corporation
3300 Plymouth Road
Ann Arbor, Michigan 48105
Mr. John M. Brueger

Boeing Company
P.O.Box 3707
Seattle, Washington 98124
Mr. J. D. Alexander

Missile Division
Chrysler Corporation
P.O.Box 2628
Detroit, Michigan 48231
Mr. John Gates

Wright Aeronautical Division
Curtiss-Wright Corporation
Wood-Ridge, New Jersey 07075
Mr. G. Kelley

Missile and Space Systems Division
Douglas Aircraft Company, Inc. (2)
300 Ocean Park Boulevard
Santa Monica, Calif. 90406
R. W. Hallet, Chief Engineer
Advanced Space Technology
Mr. A. Pisciotta, Jr.

Aircraft Missiles Division
Fairchild Hiller Corporation
Hagerstown, Maryland 21740
Mr. J. S. Kerr

General Dynamics (2)
Convair Division
5001 Kearny Villa Road
P.O.Box 1628
San Diego, Calif. 92112
Mr. E. R. Peterson, V. P. Research
and Engineering
Mr. Frank Dore

Missile and Space Systems Center
General Electric Company
Valley Forge Space Technology Center
P.O.Box 8555
Philadelphia, Pa.
Mr. F. Mezger

Advanced Engine and Technology Dept.
General Electric Company
Cincinnati, Ohio 45215
Mr. D. Suichu

Grumman Aircraft Engineering Corp.
Bethpage, Long Island
New York 11714
Mr. Joseph Gavin

Honeywell, Inc.
Aerospace Division
2600 Ridgway Road
Minneapolis, Minn.
Mr. Gordon Harms

Hughes Aircraft Co.
Aerospace Group
Centinela and Teale Streets
Culver City, Calif.
Mr. E. H. Meier, V.P. and Div.Mgr.
Research and Dev. Div.

Walter Kidde and Company Inc.
Aerospace Operations
567 Main Street
Belleville, New Jersey
Mr. R. J. Hanville
Dir. of Research Engr.

Ling-Temco-Vought Corporation
Astronautics
P.O.Box 5907
Dallas, Texas 75222
Mr. Garland Whisenhunt

Lockheed Missiles and Space Co.
Attn:-Technical Information Center
PO Box 504
Sunnyvale, California 94088
Dr. Y. C. Lee

Lockheed Propulsion Co. (2)
P.O.Box 111
Redlands, Calif. 92374
Mr. H. L. Thackwell
Mr. J. E. Fitzgerald

The Marquardt Corporation (2)
16555 Saticoy Street
Van Nuys, Calif. 91409
Mr. Warren P. Boardman, Jr.
Mr. S. Minton

Baltimore Division
Martin Marietta Corp.
Baltimore, Maryland 21203
Mr. John Calathes (3214)

Denver Division (2)
Martin Marietta Corp.
P.O.Box 179
Denver, Colorado 80201
Mr. J. D. Goodlette (A-241)
Mr. A. J. Kullas

Orlando Division
Martin Marietta Corp.
Box 5837
Orlando, Florida
Mr. J. Ferm

McDonnell Aircraft Corp. (2)
P.O.Box 516
Municipal Airport
St. Louis, Missouri 63166
Mr. R. A. Herzmark
Mr. R. E. Martens

Rocket Research Corporation
520 South Portland Street
Seattle, Washington 98108
Mr. Foy McCullough, Jr.

Space and Information Systems Div.
North American Aviation, Inc.
12214 Lakewood Blvd.
Downey, California 90241
Mr. H. Storms

Rocketdyne (Library 586-306)
North American Aviation, Inc.
6633 Canoga Avenue
Canoga Park, Calif. 91304
Mr. E. B. Monteath

Northrop Space Laboratories
3401 West Broadway
Hawthorne, California 90250
Dr. William Howard

Astro-Electronics Division
Radio Corporation of America
Princeton, New Jersey 08540
Mr. S. Fairweather

Reaction Motors Division (3)
Thiokol Chemical Corporation
Denville, New Jersey 07832
Mr. Arthur Sherman
Mr. Robert Gere
Mr. Tom Seamans

Republic Aviation Corporation
Farmingdale, Long Island, New York
Dr. William O'Donnell

Space General Corporation
9200 East Flair Avenue
El Monte, Calif. 91734
Mr. C. E. Roth

Stanford Research Institute
333 Ravenswood Avenue
Menlo Park, Calif. 94025
Mr. Lionel Dickinson

TRW Systems (2)
One Space Park
Redondo Beach, Calif. 90278
Mr. D. Lee
Mr. V. Moseley

Tapco Division
TRW Incorporated
23555 Euclid Avenue
Cleveland, Ohio 44117
Mr. P. T. Angell

Thiokol Chemical Corporation
Huntsville Division
Huntsville, Alabama 35807
Mr. John Goodloe

United Technology Center
587 Methilda Avenue
P.O.Box 358
Sunnyvale, California 94088
Mr. B. Adelman

Florida Research and Development
Pratt and Whitney Aircraft
United Aircraft Corporation
P.O.Box 2691
West Palm Beach, Florida 33402
Mr. R. J Coar

Vickers Inc.
Box 302
Troy, Michigan

Sunstrand Aviation
2421 11th Street
Rockford, Illinois 61101
Mr. R. W. Reynolds

Hamilton Standard Division
United Aircraft Corp.
Windsor Locks, Conn. 06096
Mr. R. Hatch

Multi-Tech., Inc.
601 Glenoaks Blvd.
San Fernando, Calif. 91340
Mr. F. B. Cramer

Mathematical Applications Group, Inc.
180 South Broadway
White Plains, N. Y. 10605
Dr. S. Z Burnstein

Universities

Ohio State University
Dept. of Aeronautical Eng.
Columbus, Ohio 43210
Mr. R. Edse

Pennsylvania State University
Mechanical Engineering Dept.
207 Mechanical Engineering Blvd.
University Park, Pa. 16802
Mr. G. M. Faeth

University of Southern California
Department of Mechanical Engineering
University Park
Los Angeles, Calif. 90007
Dr. M. Gerstein

Princeton University
Forrestal Campus
Guggenheim Laboratories
Princeton, New Jersey 08540
Dr. D. Harrje

University of Wisconsin
Mechanical Engineering Department
1513 University Avenue
Madison, Wisconsin 53705
Dr. P. S. Myers

University of Michigan
Aerospace Engineering
Ann Arbor, Michigan 48104
Dr. J. A. Nicholls

University of California (2)
Department of Chemical Engineering
6161 Etcheverry Hall
Berkeley, Calif. 94720
Dr. A. K. Oppenhiem
Dr. R. Sawyer

Purdue University
School of Mechanical Engineering
Lafayette, Indiana 47907
Dr. J. R. Osborn

Sacramento State College
Engineering Division
60000 J. Street
Sacramento, Calif. 95819
Dr. E. H. Reardon

Massachusetts Institute of Technology
Department of Mechanical Engineering
Cambridge, Mass. 02139
Dr. T. Y. Toong

Illinois Institute of Technology
RM 200 M.H.
3300 S. Federal Street
Chicago, Illinois 60616
Dr. T. P. Torda

Polytechnic Institute of Brooklyn
Graduate Center
Route 110
Farmingdale, New York
Dr. V. D. Agosta

Georgia Institute of Technology
Atlanta, Georgia 30332
Dr. B. T. Zinn

APPENDIX A

COMPUTER PROGRAM LISTING

```
      PROGRAM PRESS(INPUT,OUTPUT,TAPE 5=INPUT,TAPE 6=OUTPUT)
C          TRANSIENT PRESSURE HISTORY PROGRAM
C
      COMMON /A/       TFP(2),TAU(2),TAUF(2),TAUS(2),XM(2),GAM(2),TG(2),
     1PG(2),      M(2),GEVAP(2),X1(2),XR(4,2),     ROL(2),CPL(2),TO(2)
      COMMON /ABCDEF/X(4,500,2),T(4,500,2),P(4,500,2),R(4,500,2)
      DIMENSION PV(10), TD(10),TAG(2),PVW(2),PVF(4),TDK(4)
      DIMENSION W1(20,2),T1(20,2),W(500,2)
      DIMENSION TA(4),CPLA(4),G(2),GCOND(2),XMNOZ(2),TQ(2)
      DIMENSION PG1(2)
      DIMENSION ROP(2)
      DATA (ROP(1)=89.93),(ROP(2)=56.32)
      DATA ((PV(I),I=1,9)=389.29,720.,1324.8,2128.32,2733.12,4419.36,
     15561.28,6946.56,10673.28)
      DATA ((TD(I),I=1,9)=471.84,490.,510.,530.,540.,560.,570.,580.,610.
     1)
      DATA ((PVF(I),I=1,4)=79.2,300.96,720.,1051.2)
      DATA ((TDK(I),I=1,4)=474.,528.,564.,582.)
      DATA ((CPLA(I),I=1,4)=.3667,.3696,.3752,.3825)
      DATA ((TA(I),I=1,4)=524.8,530.,540.,550.)
    1 READ(5,9000) NN,M(1),M(2),NSTOP,NOW
        DO 2 L=1,NN
        DO 2 J=1,NSTOP
      X(L,J,1)=0.
      X(L,J,2)=0.
      T(L,J,1)=0.
      T(L,J,2)=0.
      P(L,J,1)=0.
      P(L,J,2)=0.
      R(L,J,2)=0.
    2 R(L,J,1)=0.
      READ(5,9005) W(1,1),W(1,2),TFP(1),TFP(2),TAUF(1),
     1TAUF(2),TAUS(1),TAUS(2),XM(1),XM(2),GAM(1),GAM(2),TG(1),TG(2),
     2PG(1),PG(2),PVW(1),PVW(2),ASTAR,VC,AC,ALPHA,DELTN,(XR(I,1),I=1,NN)
     3,(XR(I,2),I=1,NN)
C
      READ(5,9010)(R(I,1,1),I=1,NN)
      READ(5,9010)(R(I,1,2),I=1,NN)
      READ(5,9010)(T(I,1,1),I=1,NN)
      READ(5,9010)(T(I,1,2),I=1,NN)
      READ(5,9005)(W1(I,1),I=1,NOW)
      READ(5,9005)(W1(I,2),I=1,NOW)
      READ(5,9005)(T1(I,1),I=1,NOW)
      READ(5,9005)(T1(I,2),I=1,NOW)
 9000 FORMAT(6I6)
 9005 FORMAT(6E12.8)
 9010 FORMAT(4E12.8)
C          COMPUTE INITIAL CONDITIONS
           RC = 1545.
```

```
      GCOND(1)=0.
      GCOND(2)=0.
           CONST1= 4.*ALPHA*DELTN*3.1415/SQRT(6.2831853*RC/32.2)
           CONST2= 3.*ALPHA*DELTN/SQRT(6.2831853*RC/32.2)
           CONST3= CONST2*AC/3.
           CONST4 = ASTAR*SQRT(32.2/1545.)*DELTN
      NPAGE=1
C
      TIME1=0.
       TIME=0.
      N22=NOW-1
          NSTOP = NSTOP+1
      TAG(1)=0.
      TAG(2)=0.
      DT1000=DELTN*1000.
C
CC          SELECT THE CORRECT PROBLEM
C
            NPP = 0
            NPF = 0
            IF(M(1).EQ.0) NPF = 2
            IF(M(2).EQ.0) NPF = 1
            IF(NPF .EQ. 0) NPF=3
            IF(M(1).EQ.M(2)) NPF =4
            IF((M(1).LE.M(2)).AND.(M(1).GE.1))      N=1
            IF((M(2).LE.M(1)).AND.(M(2).GE.1))      N=2
       IF(NPF.LT.3) N=NPF
C
CC          THE TIME LOOP
C
            DO 1000 L=1,NSTOP
      TAG(N)=0.
               GEVAP(1) =0.
               GEVAP(2) =0.
                  X1(1) =0.
                  X1(2) =0.
      LX=L
       IF(NPF.NE.4) GO TO 205
   50 N=1
      TAG(N)=0.
       L =L-M(1)+1
      IF((LX.GE.1).AND.(M(1).GT.0)) GO TO 205
  100 N=2
      TAG(N)=0.
      LX=L-M(2)+1
      IF((LX.GE.1).AND.(M(2).GT.0)) GO TO 205
      GO TO 800
  205 BB=SQRT(XM(N))
      DO 700 NNN=1,LX
      J=L -NNN+1
      CC=W(J,N)
       DO 700 I=1,NN
       IF(N.EQ.1) GO TO 250
       DO 251 K=1,3
      IF((T(I,J,2).GE.TDK(K)).AND.(T(I,J,2).LE.TDK(K+1))) GO TO 252
  251       CONTINUE
```

```
  252 P(I,J,2)= (PVF(K+1)-PVF(K))*(TDK(K+1)-T(I,J,2))/(TDK(K)-TDK(K+1))+
     1PVF(K+1)
      TAU(2)=425.8
       IF(T(I,J,2).LT.140.) ROL(2)= 68.64*T(I,J,2)
       IF(T(I,J,2).GE.140.) ROL(2)= -.03158*T(I,J,2)+73.06
C
          CPL(2) = .00025*T(I,J,2)+.56
C
C
C
           GO TO 31
  250      CONTINUE
           IF(T(I,J,1).LT.471.84) GO TO 280
C
           DO 260 K=1,8
           IF(T(I,J,1).GE.TD(K) .AND. T(I,J,1).LE.TD(K+1)) GO TO 270
  260      CONTINUE
  270 P(I,J,1)= (PV(K)-PV(K+1))*(TD(K+1)-T(I,J,1))/(TD(K+1)-TD(K))+PV(K+
     11)
           GO TO 290
  280      P(I,J,1) = 6.158*T(I,J,1)-2624.05
C
  290      TAU(1) = 178.
C
       IF( T(I,J,1).LT. 140.4) ROL(1)= 122.49
       IF((T(I,J,1).GE.140.5).AND.(T(I,J,1).LT.471.84)) ROL(1)=-.08433*
     1T(I,J,1)+134.33
       IF(T(I,J,1).GE.471.84) ROL(1)=-.07934*T(I,J,1)+131.98
            IF(T(I,J,1).GE.524.8) GO TO 300
       IF((T(I,J,1).GE.471.84).AND.(T(I,J,1).LT.524.8)) CPL(1)=.0002325*
     1T(I,J,1)+.2446
       IF((T(I,J,1).GE.105.91).AND.(T(I,J,1).LT.471.84)) CPL(1)=.0004909
     1*T(I,J,1)+.0569
       IF( T(I,J,1).LT.105.91) CPL(1)= .00125*T(I,J,1)-.02349
        GO TO 310
  300      DO 305 K=1,3
      IF((T(I,J,1).GE.TA(K)).AND.(T(I,J,1).LE.TA(K+1))) GO TO 307
  305      CONTINUE
  307 CPL(1)= (CPLA(K)-CPLA(K+1))*(TA(K+1)-T(I,J,1))/(TA(K+1)-TA(K))+
     1 CPLA(K+1)
  310      CONTINUE
      IF(X(I,J,N).GT.1.) GO TO 312
       G(N) = ((P(I,J,N)-PG(N))*R(I,J,N)**2/SQRT(T(I,J,N)))* CONST1
       G(N) =  G(N)*BB
        IF(G(N).LT.0.) G(N)=0.
       GO TO 316
  312 G(N)=0.
  316  TOG =(G(N)*CC*XR(I,N)/(ROP(N)*R(I,1,N)**3))*.2387
       GEVAP(N) = GEVAP(N)+ TOG
       TAG(N) = TAG(N)+ TOG*T(I,J,N)
      IF(X(I,J,N).GT.0.) GO TO 315
          IF(P(I,J,N).LE.PG(N)) GO TO 315
      IF(TFP(N).EQ.T(I,J,N)) GO TO 315
      R(I,J+1,N) = R(I,J,N)*(1.-      BB*(P(I,J,N)-PG(N))*CONST2/(ROL(N)
     1*SQRT(T(I,J,N))*R(I,J,N)))**.3333
           GO TO 320
```

```
      R(I,J+1,N) = R(I,J,N)
      IF(X(I,J,N).GT.0.) GO TO 360
      IF(P(I,J,N).GT.PG(N)) GO TO 340
      T(I,J+1,N)=T(I,J,N)
      GO TO 350
  340 T(I,J+1,N)=T(I,J,N)-CONST2*TAU(N)*(P(I,J,N)-PG(N))/(ROL(N)*CPL(N)*
     1R(I,J,N)*SQRT(T(I,J,N)))*BB
      IF(T(I,J+1,N).LT.TFP(N)) T(I,J+1,N)=TFP(N)
  350 X(I,J+1,N)= X(I,J,N) + (G(N)*TAUS(N)/(ROL(N)*R(I,J,N)**3*TAUF(N)))
     1*B387
      GO TO 370
  360 T(I,J+1,N)=TFP(N)
      GO TO 350
                                    CONTINUE
  370 CONTINUE


      DO 500 K=1,N22
      IF(TIME1.GE.T1(K,N) .AND. TIME1 .LE. T1(K+1,N)) GO TO 510
  500 CONTINUE
  510 R(J+1,N)=(W1(K+1,N)-W1(K,N))*(T1(K+1,N)-TIME1)/(T1(K,N)  -T1(K+1,N
     1))+W1(K+1,N)
          IF(NPF.EQ.1) GO TO 800
          IF(NPF.EQ.2) GO TO 800
          IF(NPF.EQ.3) GO TO 710
         IF((NPF.EQ.4).AND.(N.EQ.2)) GO TO 800
          IF((NPF.EQ.4).AND.(N.EQ.1)) GO TO 100
  710     IF(N.EQ.1) MPF=2
          IF(N.EQ.2) MPF=1
          IF(M(MPF).EQ.L) NPF=4
          IF(NPF.NE.4) GO TO 800
      IF(MPF.EQ.2) GO TO 100
      IF(MPF.EQ.1) GO TO 50
      CONTINUE

          IF(NPF.EQ.4) N=1
      GCOND(N)=((PG(N)-PVW(N))*CONST3/SQRT(TG(N)))*BB
      IF(GCOND(N).LT.0.) GCOND(N)=0.
      XMNOZ(N) = (PG(N)/SQRT(TG(N)))*CONST4*BB*SQRT(GAM(N)*(2./(GAM(N)+
     1 1.))**((GAM(N)+1.)/(GAM(N)-1.)))
      TQ(N)= ( TAG(N) +VC*XM(N)*PG(N)/RC     -GCOND(N)*TG(N)-XMNOZ(N)*TG(
     1N))/(GEVAP(N)+VC*XM(N)*PG(N)/(RC     *TG(N))-GCOND(N)-XMNOZ(N))

C     TQ(N)=GEVAP(N)*RC*TQ(N)/(VC*XM(N))-RC*TQ(N)*GCOND(N)/(VC*XM(N))
      1-RC*TQ(N)*XMNOZ(N)/(VC*XM(N))+PG(N)*TQ(N)/TG(N)
      PG1(N)=PG(N)/144.

          IF(NPF.NE.4) GO TO 820
          IF((NPF.EQ.4).AND.(N.EQ.2)) GO TO 815
           N=2
           GO TO 810
  815 PGTOTL=PG1(1)+PG1(2)
          GO TO 825
  820 PGTOTL=PG1(N)
```

```
 825 IF(NPAGE .EQ. 1) WRITE(6,2000)
     IF(NPF .EQ. 4) GO TO 900
     IF(N .EQ. 1) GO TO 920
     WRITE(6,2010) TIME,PG1(2),GEVAP(2),GCOND(2),TG(2)
     NPAGE=NPAGE+1
     IF(NPAGE.GE.60) NPAGE=1
     GO TO 990
 920 WRITE(6,2020) TIME,PG1(1),GEVAP(1),GCOND(1),TG(1)
     NPAGE=NPAGE+1
     IF(NPAGE.GE.60) NPAGE=1
     GO TO 990
 900 WRITE(6,2030)  TIME,PG1(1),PG1(2),GEVAP(1),GEVAP(2),GCOND(1),GCOND
    1(2),TG(1),TG(2)
     NPAGE=NPAGE+1
     IF(NPAGE.GE.60) NPAGE=1
 990 CONTINUE
2000 FORMAT(1H1,4X,4HTIME,9X,5HPG(1),8X,5HPG(2),8X,8HGEVAP(1),5X,8HGEVA
    1P(2),5X,8HGCOND(1),5X,8HGCOND(2),5X,5HTG(1),8X,5HTG(2))
2010 FORMAT(1H ,E13.4,13X,E13.4,13X,E13.4,13X,E13.4,13X,E13.4)
2020 FORMAT(1H ,E13.4,E13.4,13X,E13.4,13X,E13.4,13X,E13.4)
2030 FORMAT(1H ,9E13.4)
3000   CONTINUE
      TG(1)=TQ(1)


      TG(2)=TQ(2)
     TIME=TIME+DT1000
     TIME1=TIME1+DELTN
1000   CONTINUE
       GO TO 1
     END
```